Chapter 4
Mathematical Modeling: Approaches for Model Solution

Auli Niemi, Zhibing Yang, Jesus Carrera, Henry Power, Christopher Ian McDermott, Dorothee Rebscher, Jan Lennard Wolf, Franz May, Bruno Figueiredo and Victor Vilarrasa

Abstract The governing equations and mathematical models describing CO_2 spreading and trapping in saline aquifers and the related hydro-mechanical and chemical processes were described in Chapt. 3. In this chapter, the focus is on methods for solving the relevant equations. The chapter gives an overview of the different approaches, from high-fidelity full-physics numerical models to more simplified analytical and semi-analytical solutions. Specific issues such as modeling coupled thermo-hydro-mechanical-chemical processes and modeling of small-scale processes, such as convective mixing and viscous fingering, are also addressed.

A. Niemi (✉) · Z. Yang · B. Figueiredo
Department of Earth Sciences, Uppsala University, Villavägen 16,
75236 Uppsala, Sweden
e-mail: Auli.Niemi@geo.uu.se

Z. Yang
e-mail: zhibing.yang@hyd.uu.se

B. Figueiredo
e-mail: bruno.figueiredo@geo.uu.se

J. Carrera · V. Vilarrasa
Groundwater Hydrology Group (GHS UPC-CSIC), Institute of Environmental Assessment and Water Research (IDAEA), Spanish National Research Council (CSIC), Barcelona, Spain
e-mail: jesus.carrera.ramirez@gmail.com

V. Vilarrasa
e-mail: victor.vilarrasa@upc.edu

H. Power
Department of Mechanical Engineering, School of Mechanical, Materials, Manufacturing Engineering and Management, The University of Nottingham, University Park, Nottingham NG7 2RD, UK
e-mail: Henry.Power@nottingham.ac.uk

C.I. McDermott
School of Geoscience, Edinburgh Collaborative of Subsurface Science and Engineering (ECOSSE), University of Edinburgh, Edinburgh, UK
e-mail: cmcdermo@staffmail.ed.ac.uk

A. Niemi et al. (eds.), *Geological Storage of CO_2 in Deep Saline Formations*,
Theory and Applications of Transport in Porous Media 29,
DOI 10.1007/978-94-024-0996-3_4

Finally, illustrative examples of modeling real systems, with different types of modeling approaches, are presented.

4.1 Different Approaches for Modeling CO_2 Geological Storage

Zhibing Yang, Auli Niemi and Jesus Carrera

The previous chapter has provided the mathematical description of the processes involved in geological storage of CO_2 in deep saline formations. These descriptions result in a set of governing partial differential equations which need to be solved together with appropriate initial and boundary conditions relevant to the systems to be modeled. This chapter discusses modeling approaches to solve these equations with emphasis on modeling large-scale systems, whose goals can range from theoretical questions, such as questions related to CO_2 dissolution or reservoir deformation, to practical issues like operational management, site screening, capacity estimation and risk assessment. This requires taking into account relevant physical processes and obtaining output from the model solutions for quantities and their uncertainties regarding issues like CO_2 mass inventory, CO_2 plume extent and pressure buildup.

As indicated by the mathematical representations in Chap. 3, CO_2 storage modeling is complicated by the presence of several multiphase flow regimes, coupled to other processes, and nonlinearity as well as parameter heterogeneity at several spatial scales, which generally hinders exact solutions. Therefore, approximate solutions often need to be sought for practical models. Generally, approximate solutions can be achieved by system simplification and/or numerical discretization (Nordbotten and Michael 2011) and may be categorized into analytical (and semi-analytical) and numerical solutions. The former are easy to use and provide insight into the nature of the problem and its solution. However, in many cases, numerical approximations are also needed because they are versatile, able to treat various boundary conditions and also to handle complex geomechanical and geochemical processes and their coupling.

D. Rebscher · J.L. Wolf · F. May
Bundesanstalt fuer Geowissenschaften und Rohstoffe (BGR), Hannover, Germany
e-mail: Dorothee.Rebscher@bgr.de

J.L. Wolf
e-mail: JanLennard.Wolf@bgr.de

F. May
e-mail: franz.may@bgr.de

In this section, we categorize the different modeling approaches for CO_2 storage into (1) high-fidelity hydrodynamic modeling, (2) reduced-physics modeling, (3) analytical modeling and (4) other modeling approaches. It can be noted that sometimes it is optimal if a combination of different approaches is used for modeling the complex system, to obtain an integrated understanding.

4.1.1 High-Fidelity Hydrodynamic Modeling

The high-fidelity hydrodynamic modeling approach refers here to numerical modeling in which three-dimensional balance equations describing multiphase flow and transport processes at a suitable scale are solved with sufficient accuracy and minimum degree of system simplification. In this kind of modeling, available geological information concerning the reservoir reservoir rock properties and boundaries as well as geometrical and structural features is taken into account to a degree that is the maximum computationally affordable. In other words, a minimum set of simplifications in terms of the hydrodynamic behavior and system characteristics is applied.

In order to solve the three-dimensional mass and energy balance equations, the spatial domain is discretized into a finite number of nodes/elements or cells and the continuous partial differential equations (PDEs) are converted to discrete equations typically using the finite differences method (FDM), the finite element method (FEM) or the finite volumes method. Eventually, the PDEs are represented by a set of (non-)linear algebraic equations at discrete time steps, which can be solved to yield numerical solutions at each node/element for a desired simulation period.

4.1.1.1 Simulation Codes for Hydrodynamic Modeling of CO_2 Storage

Historically, many simulation codes have been developed by petroleum engineers and groundwater hydrologists to obtain numerical solutions to the multiphase flow and transport problems. During the last decade, many of these codes have been extended to incorporate the ability to simulate the CO_2 storage system, since essentially the same basic governing equations are used to represent the system and only the fluid properties and associated phase behaviors need to be changed. Each code has different features that are included. The codes can be broadly divided into two categories: research codes [e.g. TOUGH2 (Pruess et al. 1999), CODE_BRIGHT (Olivella et al. 1996), PFLOTRAN (Hammond et al. 2007), OpenGeoSys (Kolditz et al. 2012a), GPRS (Cao 2002)] and commercial codes [e.g. ECLIPSE (Schlumberger 2012)]. Here we give an example for each category, while a complete list of codes is not pursued.

One of most widely used research codes is TOUGH2 (Pruess et al. 1999), developed by Lawrence Berkeley National Laboratory. It is a general-purpose

simulation code for non-isothermal, multi-component, multi-phase fluid flow in porous and fractured media. It employs integral finite difference for spatial discretization, and uses fully implicit, first-order finite differences for temporal discretization. The non-linear equations for each time step are solved using a Newton–Raphson iterative method with adaptive time step size. It has been coupled to a reactive transport simulator [TOUGHREACT (Xu et al. 2014)], using the formulation of Saaltink et al. (1998), described in Sect. 3.4. ECO2N (Pruess 2005) is a fluid property module for the TOUGH2 simulator for applications to geologic sequestration of CO_2 in saline aquifers. It describes the thermodynamics and thermophysical properties of H_2O–NaCl–CO_2 mixtures, and accurately reproduces fluid properties for the temperature, pressure and salinity conditions of interest for geological sequestration (10 °C $\leq$ T $\leq$ 110 °C; P $\leq$ 600 bar; salinity up to full halite saturation) and ECO7CMA (Freifeld et al. 2013) have extended the properties to even greater depths and larger temperatures. Phase conditions considered include a single (aqueous or CO_2-rich) phase, as well as two-phase mixtures. Local equilibrium solubility is applied to treat phase partitioning between the aqueous and the CO_2-rich phase as well as to handle dissolution or precipitation of salt. An option for modeling associated changes of porosity and permeability is also included. In ECO2N, no distinction is made with regard to whether the CO_2-rich phase is liquid or gas. In ECO2M (Pruess 2011), an enhanced version of ECO2N, all possible phase conditions for brine–CO_2 mixtures, including transitions between super- and sub-critical conditions, and phase change between liquid and gaseous CO_2 are described, which allows for more accurate modeling of CO2 leakage to the shallow subsurface. Essentially, CODE_BRIGHT incorporates the same suite of processes but its coupling to mechanical deformation is direct. It is also coupled to reactive transport (Saaltink et al. 2004) and was modified as part of the MUSTANG project to incorporate CO_2 as a fluid phase.

One of the extensively used simulators in the petroleum industry is ECLIPSE (Schlumberger 2012). It is a fully implicit, three dimensional, general purpose simulator and has two modules: one for black oil simulation (E100) and the other for compositional simulation (E300). E100 assumes three components, water, oil and gas in a three-phase system of liquid, gas and gas in solution. When applied to the CO_2 storage system, E100 essentially uses a gas–oil system with the oil phase given the brine properties and the gas phase given the CO_2 properties (Singh et al. 2010). E300 is a compositional simulator with a cubic equation of state and features like pressure-dependent permeability values. E300 includes an option called CO2STORE which can handle mutual solubility of CO_2 and water and accurately calculate the fluid properties (density, viscosity, compressibility, etc.) of pure and impure CO_2 as a function of temperature and pressure. It also includes functionality to describe the dry-out and salt precipitation phenomena. Accurate calculations of fluid properties and mutual solubility are required for accurate hydrodynamic modeling of CO_2 storage system. However, it is worth noting that compositional

simulations with a sophisticated equation of state, though very accurate in representation of the fluid properties, will correspond to much more expensive computational burden than that in black oil simulations (Hassanzadeh et al. 2008). An efficient thermodynamic model (Hassanzadeh et al. 2008) has been developed to reproduce the PVT data for the CO_2–brine mixture to be used in black-oil simulations for saving computational time.

4.1.1.2 An Illustrative Example

We here present an example of full-physics hydrodynamic modeling, using the TOUGH2 model, for the purpose of illustrating the flow regimes and the spatial distributions of quantities of practical interest such as gas saturation and pressure perturbation. A 'disk-shaped', vertically bounded formation is considered. Some of the main parameters for the simulation are summarized in Table 4.1. The parameters are chosen to represent typical scenarios of industrial scale CO_2 storage, except that formation water salinity is ignored in this example. The radial extent is set to a large value and is infinite acting for the example considered here. CO_2 storage is simulated as injection along a vertical well perforated through the whole formation thickness.

Figure 4.1 presents the simulated spatial profile of vertically averaged CO_2 saturation and pressure increase for the example CO_2 injection scenario, which can be considered representing an industrial scale CO_2 injection. As can be seen in Fig. 4.1, there exists a dry-out zone (free of aqueous phase) around the injection well. In this dry-out zone all water has been either displaced outwards or vaporized into the CO_2-rich (gas) phase. In this example, salinity is not considered. When salinity is considered, the salt that is originally dissolved in the brine would have precipitated in the dry-out zone and would thus reduce the porosity and permeability. The radius of dry-out zone is on the scale of $\sim$100 m at the end of the injection period (say e.g. 50 years). Surrounding the dry-out zone is a region where the gas phase and the aqueous phase co-exist. The radius of this two-phase flow region is typically several kilometers at the end of the injection period. Outside of the two-phase region only brine exists with single phase brine flow.

Table 4.1 Modeling parameters for the illustrative example

Parameter	Value and unit	Parameter	Value and unit
Initial pressure	160 bars	Temperature	45 °C
Permeability	100 mD	Porosity	0.12
Thickness	50 m	Injection time	50 years
Res. brine sat.	0.3	van Genuchten param. m	0.41
Entry pressure	9983 Pa	Salt mass fraction	0.0
Radial extent	250 km	Injection rate	1.0 Mt/a

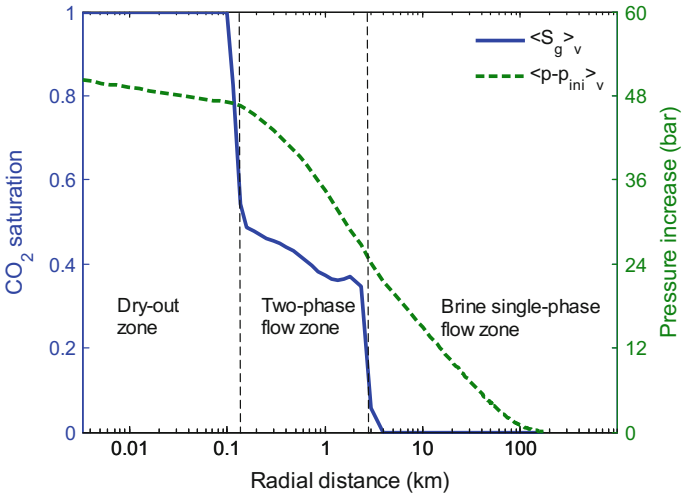

Fig. 4.1 Radial profile of CO_2 saturation and pressure increase (vertically averaged) at 50 years for an injection scenario with rate 1 Mt/a based on the high-fidelity modeling of an ideal disk-shaped infinite-acting aquifer using TOUGH2/ECO2N

4.1.1.3 Application Examples

Examples of using the TOUGH2 simulator and its extensions for obtaining numerical solutions to study varying aspects of geological storage of CO_2 are widely available in the literature, and several examples are presented throughout this book. For example, Zhou et al. (2010) performed a basin-scale simulations for multiple-site CO_2 injection in the Mount Simon aquifer in the Illinois Basin. They simulated CO_2 injection with a rate of 5 Mt/year/well and a total number of 20 wells, given the thick Mount Simon aquifer (300–730 m) confined by the low-permeability Eau Claire caprock. Both the plume-scale processes (i.e. hydrodynamic interactions between supercritical CO_2 and formation brine) and the basin-scale processes (i.e. large-scale pressure build-up and brine migration) were modeled. Numerical solutions were obtained with regard to CO_2 mass distribution, CO_2 plume sizes and fluid pressure changes for the aquifer as a whole, which can facilitate evaluation of the injection strategies and the large-scale hydrogeological impact. Yang et al. (2015) and Tian et al. (2016) presented a comprehensive simulation workflow, where TOUGH2/ECO2N is used together with simpler models (semi-analytical solutions and vertical equilibrium models), and estimated the CO_2 storage capacities of the Baltic Sea Basin and the South Scania site, given the constraints due to pressure build-up and long-term CO_2 containment.

The ECLIPSE reservoir simulator package has also been applied in many studies for numerical solutions of modeling CO_2 storage. For instance, Juanes et al. (2006) used the ECLIPSE black oil simulator to investigate the role of relative permeability hysteresis on CO_2 residual trapping for both a synthetic geological formation and a

more realistic geological model (the PUNQ-S3 Case Studies). Shamshiri and Jafarpour (2012) employed the compositional simulator E300 for modeling CO_2 injection and migration with the aim of developing optimized injection rate allocation for improved residual and dissolution trapping as well as decreased risk of CO_2 plume approaching leakage pathways.

4.1.1.4 Remarks on High-Fidelity Hydrodynamic Modeling

High-fidelity modeling with sophisticated numerical simulators, can yield simulation results that are the most accurate achievable, provided that all the relevant processes are considered and space and time are properly discretized. It can also serve as a benchmark for comparison when we attempt to simplify the mathematical description for gaining insight into the interplay between parameters/processes. However, CO_2 storage systems are quite complex to model with physical processes spanning a wide range of spatial and temporal scales (Nordbotten and Michael 2011). Even though simulators are continuously becoming increasingly powerful in terms of considering a multitude of physical processes and handling larger grids, there are still limitations to integrate the effect of small-scale hydrodynamic processes into large scale models (this requires upscaling, which is the subject of Chap. 5). To this end, continued development and enhancement of simulation codes continues to be important.

High-fidelity, high-resolution numerical simulations at the reservoir or basin scale require solving the 3D non-linear partial differential equations with large grids, which points to the need for a significant amount of computational power and resources. Efficient modeling and performance optimization are often pursued. Parallel computing is becoming more and more important with the need for more accurate simulation results and better computing performances. Nowadays several codes offer parallel computing options (e.g. Lu and Lichtner 2007; Zhang et al. 2008). Zhou et al. (2010), Yamamoto et al. (2009), Yang et al. (2015), and Tian et al. (2016) are examples of full basin-scale integrated modeling of CO_2 storage using parallel simulation codes.

For full basin-scale 3D models it would be restrictive, if not impossible, to incorporate the multi-scale heterogeneity and scale-dependent processes. Even though computers are becoming more and more powerful, the computational resources needed for accurate solutions for practical basin-scale modeling of CO_2 storage are often beyond the given computational capabilities. Besides, there will be a lack of geological information for the parameters that are used in fine spatial resolution models. Oftentimes, simplification through parameter averaging or process upscaling is unavoidable.

Finally, it should be pointed out that different numerical simulators may show discrepancies because of factors such as the way fluid properties are calculated or differences in the numerical solution or gridding and time stepping. In practice, differences in the way different modelers interpret the setting of a given problem may be even more important. In order to understand the impact of both numerical

and modeling differences it is important to perform code inter-comparison studies of model solutions for benchmark problems (Pruess et al. 2004; Class et al. 2009; Nordbotten et al. 2012).

4.1.2 Reduced-Physics Modeling

As pointed out in the previous section, high-fidelity full physics modeling may not always be viable or necessary. In such situations, system simplification can be made through reduction of the number of processes considered by keeping only those that are dominant and essential for the objectives of the study. System simplifications can also be done by replacing the complex domain geometries with simpler ones and reducing the dimension of the model (e.g. from 3D to 2D and even 1D). A set of seven different system simplifications for practical modeling of CO_2 storage is summarized and discussed in Celia and Nordbotten (2009). Invoking subsets of simplifications, we can modify the general governing equations to obtain a new and simpler set of equations which may render analytical and/or semi-analytical solutions or considerably easier numerical solutions. This can bring great computational benefits, especially if a Monte Carlo approach is required for uncertainty quantification (see Chap. 5).

In this section, we describe two simplified numerical modeling approaches for practical modeling of CO_2 storage. Analytical solutions are discussed in the next Sect. 4.1.3.

4.1.2.1 Vertical Equilibrium Approach

Given that for CO_2 storage projects, the lateral length scale of a storage formation is typically much larger than the thickness of the formation, it is convenient to make the so-called vertical equilibrium assumption (Lake 1989; Yortsos 1995), which is the CO_2 storage version of the Dupuit approximation. This approximation is based on the assumption that the timescale for gravity segregation is much shorter than that of lateral flow. This means that the vertical distribution of quantities, such as pressure and fluid saturation, can be defined from vertically averaged quantities (Gasda et al. 2011). To further simplify the system of analysis, it may also be convenient to assume that there exists a macroscopic sharp interface between the CO_2 and brine. This assumption may be reasonable when the capillary fringe between CO_2 and brine is very small compared to the thickness of the domain. Figure 4.2 presents a schematic showing the vertically averaged CO_2-brine system where B is the thickness of the formation, b is the thickness of the CO_2 plume, and d_B, d_M, and d_T are the distances between the datum z = 0 and the bottom surface, the macroscopic interface and the top surface, respectively.

Starting from the three-dimensional mass balance equation for phase α ($\alpha = a$ for the aqueous phase and $\alpha = g$ for the CO_2-rich, or gas, phase), which was introduced in Sect. 3.3 (Eq. 3.3.26), while neglecting dissolution, we have:

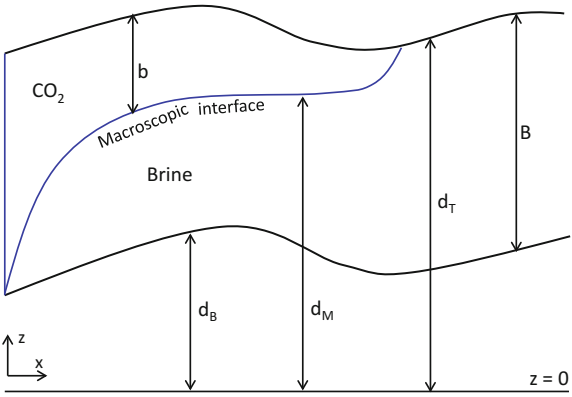

Fig. 4.2 Schematic for vertically averaged configuration of macroscopic regions of CO_2 and brine [modified after Gasda et al. (2009)]

$$\frac{\partial(\phi\rho_\alpha S_\alpha)}{\partial t} + \nabla\cdot(\rho_\alpha \mathbf{q}_\alpha) = \rho_\alpha G_\alpha. \tag{4.1.1}$$

In the above equation, ϕ is porosity, ρ_α is the fluid density of α-phase, S_α is the saturation of α-phase, $\mathbf{q}_\alpha$ is the flux calculated by Darcy's law and G_α is the source or sink term. Vertical integration of Eq. (4.1.1) for each phase over the formation thickness gives (Gasda et al. 2009):

$$\begin{aligned}&\phi\rho_a\bar{\beta}_a(B-b)\frac{\partial p_a}{\partial t} + \phi\rho_a(1-S_{ar})\frac{\partial}{\partial t}(B-b) + \nabla\cdot\rho_a\bar{\mathbf{q}}_a \\ &\quad - \rho_a q_{a,v}\big|_{d_B} + \rho_a q_{a,v}\big|_{d_T} = \int_{d_B}^{d_M}\rho_a G_a dz\end{aligned} \tag{4.1.2a}$$

$$\begin{aligned}&\phi\rho_g\bar{\beta}_g b(1-S_{ar})\frac{\partial p_g}{\partial t} + \phi\rho_g(1-S_{ar})\frac{\partial b}{\partial t} + \nabla\cdot\rho_g\bar{\mathbf{q}}_g \\ &\quad - \rho_g q_{g,v}\big|_{d_B} + \rho_g q_{g,v}\big|_{d_T} = \int_{d_B}^{d_M}\rho_g G_g dz\end{aligned} \tag{4.1.2b}$$

In Eq. (4.1.2), S_{ar} is the residual brine saturation, p_α is the fluid pressure of α-phase, $\bar{\beta}_\alpha$ is the vertically average bulk compressibility of phase α, $q_{\alpha,v}$ is the vertical component of the flux of phase α, and $\bar{\mathbf{q}}_\alpha$ is the vertically integrated horizontal fluxes for phase α which can be obtained from

$$\bar{\mathbf{q}}_a = -\frac{(B-b)\mathbf{k}}{\mu_a}\left[\nabla p_{top} + \rho_a g\nabla d_T - (\rho_a-\rho_g)g\nabla b\right] \tag{4.1.3a}$$

$$\bar{\mathbf{q}}_g = -\frac{bk^*_{r,g}\mathbf{k}}{\mu_g}\left[\nabla p_{top} + \rho_g g \nabla d_T\right] \tag{4.1.3b}$$

where $\mathbf{k}$ is the intrinsic permeability tensor, $k^*_{r,g}$ is the relative permeability of the CO_2-rich (gas) phase evaluated at gas saturation $(1 - S_{ar})$, μ_α is the viscosity of α-phase, g is acceleration due to gravity and p_{top} is the fluid pressure along the top of the formation. Under the vertical equilibrium assumption, the fluid pressure p_α in Eq. (4.1.2) is related to p_{top} according to vertical static distribution.

It must be emphasized that the above descriptions of VE assumption are limited to the scenario of primary drainage, corresponding to the CO_2 injection period. For the post-injection period, the fluid region occupied by CO_2 needs to be divided into a mobile CO_2 region and residual CO_2 region. The above Eqs. (4.1.2) and (4.1.3) also need to be reformulated to include residual trapping.

Equations (4.1.2) and (4.1.3) together describe the vertically integrated flow system in a formation and can be solved for pressure and for the thickness of the CO_2 plume with appropriate initial and boundary conditions using numerical methods such as FEM and FDM. Compared with the 3D full-physics modeling approach, the sharp-interface vertical equilibrium approach requires significantly less computational resources due to the fact that (1) the two-dimensional equations are much more efficient to solve and (2) the nonlinearities resulting from local relative permeability and capillary pressure in the 3D representation are greatly reduced (Lake 1989; Yortsos 1995; Celia and Nordbotten 2009; Gasda et al. 2009, 2011).

The effectiveness of the VE approach for exploring CO_2 injection and migration at large spatial and temporal scales has been demonstrated in a modeling study (Gasda et al. 2012) where the VE model was modified to take into account the effect of capillary fringe and convective dissolution. The study applied the modified VE modeling approach to the Johansen Formation and investigated the relative-importance of small scale processes, including residual trapping, capillary fringe and convective dissolution, on long-term CO_2 storage security. Yang et al. (2015) and Tian et al. (2016) in turn compared numerical solutions obtained by a VE model and a 3D TOUGH2 model, and demonstrated the usefulness of the VE approach. Further improvements to the VE approach are discussed by Nilsen et al. (2016), which introduces the MRST-CO2LAB family of codes that is designed to interact with oil industry codes, and Andersen et al. (2015), which explicitly acknowledges the high compressibility of CO_2 by simulating its density variations.

When the storage system is further simplified (e.g. assuming a horizontal, homogeneous formation with uniform thickness), the sharp-interface vertical equilibrium approach can also allow approximate analytical solutions for plume migration in the three-dimensional radially symmetrical or two-dimensional systems. These will be further discussed in Sect. 4.1.3.

4.1.2.2 Single-Phase Flow Modeling for Far-Field Pressure Buildup

Injection of a large volume of CO_2 induces large scale pore pressure buildup and associated change in the stress field, which may become a limiting factor for the CO_2 storage capacity. Far-field brine displacement into fresh-water aquifers or brine leakage through unplugged wells or fault zones may be induced by large-scale pressure buildup, even if the injected CO_2 is safely trapped. Here, far-field may be defined as regions outside of the CO_2 plume, i.e. the single-phase brine flow regions as indicated in Fig. 4.1.

The CO_2-brine two-phase complications are not important when the objective of the modeling study is to evaluate the far-field pressure impact and to determine the Area of Review (defined as the regulatory region surrounding the CO_2 storage where there may be detrimental effects on groundwater resources) at the regional/basin scale, given that the CO_2 plume size is relatively small compared to the spatial scale of interest. It has been shown (e.g. Chang et al. 2013; Yang et al. 2013a; Huang et al. 2014) that single-phase models may be sufficient for prediction of far-field pressure perturbation. The key point is calculating the volume of the CO_2 plume in order to know the volume of displaced brine and therefore determine the induced pressure buildup in the far-field. The volume of the CO_2 plume is not a straightforward calculation because the dependence is two-way: CO_2 density depends explicitly on fluid pressure, but fluid pressure also depends on density, because density controls the plume volume, and thus the fluid pressure through the volume of water that needs to be displaced. This nonlinear problem can be solved using an iterative scheme (Vilarrasa et al. 2010a). Single-phase flow equations are much easier to solve than multi-phase flow ones and offer significant computational advantage. For example, single-phase numerical modeling has been applied to evaluate the potential impact of CO_2 injection in the Texas Gulf Coast Basin on the shallow groundwater resources (Nicot 2008) and to estimate the pressure build-up at South Scania site in Sweden by Yang et al. (2013a). Yang et al. (2013a) also show the comparison and good agreement in predictions for far-field pressure build-up between the full two-phase simulation with TOUGH2 and the single phase with simple Theis solution (see Chap. 7). However, it should be pointed out that while the single-phase flow models are appropriate for predicting pressure buildup in the single-flow domain of the far-field, they are obviously not appropriate for pressure prediction near the CO_2 injector (which may be important for the analysis of mechanical failure) where processes and effects such as brine evaporation, viscosity contrast and two-phase flow are important.

4.1.3 Analytical Solutions

Development of analytical models for flow and transport problems in hydrogeology has been an important and continuous effort since decades ago. Analytical solutions

can provide physical insight into the balance of the physical driving mechanisms or for verifying numerical models for special cases. They are also extensively used for the interpretation of characterization tests (see Chap. 7). Even though exact analytical solutions to the general two-phase flow equations are not achievable, derivation of approximate analytical solutions with simplifying assumptions to the two-phase flow equations under certain initial and boundary conditions is still desirable. In contrast to numerical models, analytical methods allow for rapid evaluation and can be employed to study parameter sensitivity for quick site screening and evaluation. Thus, analytical solutions can be useful to support decision making concerning the operation of CO_2 injection projects and provide guidance for scenario selection for more detailed full-physics modeling (see e.g. Yang et al. 2013a, 2015). In some cases, it is also beneficial to incorporate analytical solutions in a numerical framework to form a hybrid numerical-analytical approach. An example of such approach is given in Gasda et al. (2009), where analytical solutions of sub-scale flow through leaky wells are embedded into a vertical equilibrium numerical model.

For application to CO_2 storage problems, approximate analytical solutions have been used to model CO_2-brine interface dynamics during injection (e.g. Nordbotten et al. 2005; Nordbotten and Celia 2006; Dentz and Tartakovsky 2008; Houseworth 2012; Vilarrasa et al. 2013a), pressure buildup (e.g. Vilarrasa et al. 2010a, 2013a; Mathias et al. 2011; Nordbotten et al. 2005; Nordbotten and Celia 2006; Dentz and Tartakovsky 2008; Houseworth 2012; Yang et al. 2015; Tian et al. 2016), brine leakage through abandoned wells (Cihan et al. 2011) and post-injection CO_2 plume migration that incorporate capillary trapping (Hesse et al. 2008; MacMinn and Juanes 2009; Juanes et al. 2010) and/or CO_2 dissolution (MacMinn et al. 2011). Each of the analytical solutions employs a different set of assumptions. In the following, we focus on CO_2 plume shapes and pressure buildup, and introduce some of the (semi)-analytical models.

4.1.3.1 CO_2–Brine Interface Dynamics During Injection

For the derivation of the analytical solutions describing CO_2 plume migration, both during injection and after injection, the sharp interface assumption is typically made. The abrupt interface approximation considers that the two fluids, CO_2 and brine in this case, are immiscible and separated by a sharp interface and capillary effects are usually neglected. The fluid regions occupied by CO_2 or brine are assumed to have constant saturations, written below for simplicity as 0 for the aqueous phase saturation in the CO_2 occupied region, and vice versa.

The two standard solutions for the brine interface are those of Nordbotten et al. (2005) and Dentz and Tartakovsky (2008). The former derived their solution neglecting the gravity term in the flow equation, thus emphasizing viscous dissipation, and approximating the aquifer response by Cooper Jacobs approximation (see also Chap. 7). In addition, they impose (1) volume balance, (2) gravity override

(CO_2 plume travels preferentially along the top) and (3) they minimize energy at the well. The fluid pressure applies over the entire thickness of the aquifer and fluid properties are vertically averaged. The vertically averaged properties are defined as a linear weighting between the properties of the two phases. Nordbotten et al. (2005) write their solution as a function of the mobility, ratio of relative permeability to viscosity, of each phase. For the case of an abrupt interface where both sides of the interface are fully saturated with the corresponding phase, the relative permeability is 1 and the mobility becomes the inverse of the viscosity of each phase, assumed constant. Under this conditions, the thickness of the CO_2 plume is:

$$b = B\frac{\mu_c}{\mu_w - \mu_c}\left(\sqrt{\frac{\mu_w Q_0 t}{\mu_c \phi \pi B r^2}} - 1\right) \tag{4.1.4}$$

where B is the thickness of the formation, r is the radial distance, and Q_0 is the volumetric injection rate.

Dentz and Tartakovsky (2008) derived an analytical solution by adopting complementary assumptions. That is, they invoked of the Dupuit assumption and the quasi-steady approximation for vertical equilibrium, thus neglecting vertical viscous dissipation and emphasizing buoyancy forces. They find that the thickness of the CO_2 plume, b, for radially symmetrical three-dimensions is equal to

$$b = B(1 - \Lambda_{cw}\ln[r/r_b]) \tag{4.1.5}$$

where $r_b = \sqrt{2Q_0 t/\pi\varphi B\Lambda_{cw}(e^{2/\Lambda_{cw}} - 1)}$ is the radius of the CO_2 plume at the base of the aquifer, and $\Lambda_{cw} = Q_0(\mu_a - \mu_g)/2\pi kB^2 g(\rho_a - \rho_g)$ is a dimensionless parameter that measures the relative importance of viscous and gravity forces.

It should be noted that the solution given by Eq. (4.1.5) is best in the buoyancy-dominated flow regime, that is for low injection rate, high permeability, or far from the injection well, where buoyancy dominates over viscous forces. Such conditions can be found in storage sites like Sleipner, Norway, where the reservoir has a high permeability and even though 1 Mt of CO_2 is stored annually, gravity forces dominate (Cavanagh et al. 2015). Nevertheless, such high permeability reservoirs are scarce, and since the injection rate will have to be as large as geomechanically permissible in order to achieve better CO_2 storage efficiency, viscous forces are likely to dominate in most storage sites near the injection well. Still, Eq. (4.1.5) should be the formulation of choice for prediction of CO_2 plume evolution at the regional scale.

An inherent assumption in the analytical solutions given in Dentz and Tartakovsky (2008) and Nordbotten et al. (2005) is that volumetric injection rate and the CO_2 properties (density and viscosity) are kept constant. In reality, however, the properties of CO_2 can vary significantly as the pressure changes and thus the volumetric injection rate cannot be prescribed. The compressibility of CO_2 can be one or two orders of magnitude larger than that of brine for typical injection depth. Vilarrasa et al. (2010a) proposed an iterative method to account for CO_2

compressibility in these analytical solutions. Thus, the actual mean CO_2 density and CO_2 viscosity of the plume are used, leading to more accurate estimations of the CO_2 plume position and pressure buildup than when CO_2 compressibility is neglected (Vilarrasa et al. 2013a). Further extended the solution to cases where the CO_2 density can vary in space and time as the fluid pressure evolves. A further merit of this semi-analytical solution is that it allows for an uneven distribution of mass injection rate along the vertical well. It employs vertical discretization (layers) of the formation thickness to include buoyancy flow between layers and calculates the pressure build up and interface position in a step-wise manner in time. For more details, interested readers are referred to Vilarrasa et al. (2013a).

4.1.3.2 Pressure Buildup

Injecting a large volume of CO_2 in deep saline formations causes significant pore pressure buildup near the injection well and associated change in the stress field. This may induce tensile or shear failure of the caprock (Rutqvist et al. 2008; Vilarrasa et al. 2010b) and reactivation of existing fractures or faults (Rutqvist and Tsang 2002; Streit and Hillis 2004; Cappa and Rutqvist 2011). The storage capacity of a formation is thus limited by, among other factors, the maximum allowed pressure buildup.

Pressure buildup can be easily calculated by means of a semi-analytical solution, once the interface position has been obtained, by simply integrating Darcy's law, typically assuming radial flow (Hesse et al. 2008; Mathias et al. 2011; Cihan et al. 2011; Mathias et al. 2013). Vilarrasa et al. (2010a) show that pressure buildup for a constant injection into an infinite homogeneous formation equals

$$p - p_0 = \frac{Q_0 \mu_w}{2\pi B k} \begin{cases} \ln\left(\frac{R}{r_0}\right) + \sqrt{\frac{\mu_c \phi \pi B}{\mu_w V(t)}}(r_0 - r_b) + \frac{\mu_c}{\mu_w}\ln\left(\frac{r_b}{r}\right), & r < r_b \\ \ln\left(\frac{R}{r_0}\right) + \sqrt{\frac{\mu_c \phi \pi B}{\mu_w V(t)}}(r_0 - r), & r_b \le r < r_0 \\ \ln\left(\frac{R}{r}\right), & r \ge r_0 \end{cases} \quad (4.1.6)$$

where, p is the pressure, p_0 is the initial pressure, $V(t)$ is the volume injected up to time t, and r_0 and r_b are the radii of the top and bottom of the plume, which can be obtained from Eqs. (4.1.4) and (4.1.5), respectively, for the formulations of Nordbotten et al. (2005) and Dentz and Tartakovsky (2008), discussed above. Details on these approximations, including how to acknowledge that CO_2 density varies with depth and radial distance, are discussed by Vilarrasa et al. (2010a).

It can also be seen that Eq. (4.1.6) simply represents a generalization of Thiem's solution for transient problems because $R = \sqrt{2.25 k \rho_w g t / \mu_w S_s}$ (see Sect. 7.1.3). As such, it simplifies viscous dissipation effects near the injection well, such as

vertical flow components at the plume edge or partial penetration (all analytical approximations, and most numerical solutions assume that flow is uniformly distributed along the vertical at the injection well, whereas it should concentrate at the top for low flow rates and at the bottom for high flow rates in partially penetrating wells). These effects are acknowledged by the semi-analytical solutions of Vilarrasa et al. (2013a).

4.1.4 Other Modeling Approaches

Apart from the analytical solutions and comprehensive high-fidelity numerical models discussed above, alternative methods have also been developed for modeling CO_2 migration. Most notable of these are perhaps invasion percolation (IP) models and streamline-based approaches. They are complementary to the methods discussed above and can give additional understanding to the system in special cases. A brief introduction to these methods is given below.

4.1.4.1 Invasion Percolation Approach

Invasion percolation (IP) was introduced in the 1980s (Wilkinson and Willemsen 1983) as a model for describing slow fluid displacement (i.e. negligible viscous forces) in porous media at the microscopic (pore) scale. Based on the classical percolation theory, IP takes into account the fluid transport process by considering a path of least capillary resistance. Application of the IP models requires an infinitesimal flow rate where the capillary forces dominate over the viscous forces. For typical CO_2 injection scenarios, such as the illustrative example given in Sect. 4.1.1, the pressure gradient is about 10^5 Pa/m close to the injection well but decreases to $\sim 10^3$ Pa/m in the two-phase flow zone. Upon comparison with the entry capillary pressure of $\sim 10^4$ Pa, this means that, at the sub-meter scale the capillary dominance condition will usually be satisfied. In a general case, one can calculate the dimensionless capillary number to check the relative importance of capillary forces over viscous forces (Lenormand et al. 1988). IP models are particularly well suited to study the effects of small scale heterogeneity. In fact, Kueper and McWhorter (1992) applied the IP model at the macroscopic scale to perform large-scale averaging of capillary pressure functions for unsaturated flow.

IP have been used for CO_2 storage simulations. A macroscopic IP model (Yang et al. 2013b) was used to upscale capillary pressure and relative permeability relationships for CO_2 migration in a multimodal heterogeneous field. An IP simulator has also been developed (Singh et al. 2010) and applied to the Sleipner Layer 9 benchmark problem.

4.1.4.2 Streamline-Based Approach

Streamline-based models have been also developed to simulate CO_2 storage (Jessen et al. 2005; Obi and Blunt 2006). In streamline-based approaches an operator splitting method is typically used. The basic idea is to decouple the advective from dispersive/reactive terms in the saturation transport equation, transforming a three-dimensional system into a series of one-dimensional equations. At each time step, the pressure equation and flow velocity fields are solved and streamlines are traced on the underlying grid. Then one-dimensional advective transport of saturation and concentration is numerically solved along the streamlines, possibly including exchange with adjacent streamlines explicitly in time. After accounting for the dissolution and reactions, the saturation and concentration can then be mapped to the underlying grid. These are then used to solve for the total flow (aqueous plus CO_2 phases). The two steps (flow computations and saturation transport) are repeated through discrete time steps. The streamline-based approach has been demonstrated, for example, by simulation of CO_2 storage in a highly heterogeneous million-grid-block model of a North Sea reservoir (Obi and Blunt 2006). The main advantage of the streamline-based approach lies in its computational efficiency. While the method is usually solved under the assumptions of incompressible flow and negligible capillary pressure, neither one is strictly needed and may be a significant source of error for CO_2 transport prediction in some cases.

4.2 Modeling of the Coupled Processes

Christopher Ian McDermott

4.2.1 Introduction

During CO_2 injection into a saline aquifer, Thermal, Hydraulic, Mechanical and Chemical (THMC) processes are operating on the system (see Chap. 2, 3). These processes also influence each other. We commonly use the term coupled processes when the parameters of one process depend on the solution of another one and with coupled THMC processes we mean the couplings between these four processes.

To attempt to model the behavior of such a system some estimation as to the importance of different processes and their interaction needs to be made. It is not possible to model in detail every single process and phenomena present. Therefore, decisions need to be taken which processes and phenomena are included and how the model is to represent the coupling between the processes. Key decision in the modeling process is not so much finding the most accurate mathematical representation of the system, but the decision which processes can be left out without losing key characteristics of the system. Below we will briefly discuss the

importance of coupled processes, the basis behind their division and the numerical methods for solving these processes and their coupling.

4.2.2 *Brief Overview of Coupled Processes*

Several researchers have described a number of physical phenomena as a result of the coupled THMC processes interacting with one another, a key pioneering paper being (Tsang 1991). Since then, there have been several hundreds of publications on this topic. The interaction of coupled processes leading to physical phenomena is illustrated in Fig. 4.3 (see also Fig. 2.3 in Chap. 2 for the basic concept of coupled processes in CO_2 geological storage). The diagram in Fig. 4.3 demonstrates the fact that all the key processes are linked via material behavior and coupled in various ways. This material behavior (physically observable phenomena), leads to a measureable, observable change in the properties of the continuum as a response to the change of two or more of the field variables of temperature, pressure, stress or chemistry. This behavior is also influenced in the storage settings we are considering by the complex three dimensional heterogeneous geology which the saline aquifer forms part of. The geology defines the distribution of the different facies present and their associated material parameters. We can expect that all of the physical phenomena illustrated in the figure below, will be operating in a caprock during CO_2 geological storage.

As the material characteristics change the interaction of the processes may either amplify the effect of a certain phenomenon, or diminish it through a feedback

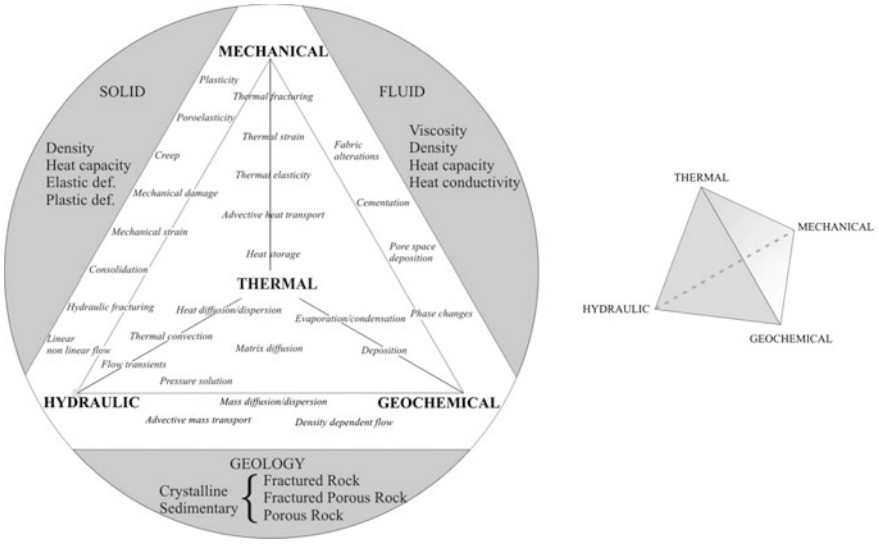

Fig. 4.3 Illustration of coupled processes effects

mechanism. For instance, temperature impacts fluid flow through viscosity, with increasing temperature leading to lower viscosity, which in turn leads to increased fluid flow and to an increased control of the fluid temperature on the system. To try to investigate a system by only considering one of the processes leads to an oversimplified representation.

Modeling systems such as these requires an understanding of the key processes operating, the scale at which the processes are operating, the magnitude of the fields gradients present (fluid pressure, temperature, stress, chemical concentration) and the different strata through which the processes are operating. For example, in flow dominated systems advective heat transport may be much more rapid than the convective transport of heat.

Any modeling approach also needs to take the different spatial and temporal scales into account. Complicated balance equations describing pore level processes may be solvable but must be up-scaled (see Chap. 5) to be useful for large scale modeling of a CO_2 storage site. Methods of solution include the application of multiple mesh approaches, adaptive mesh refinement, and hybrid analytical and numerical solutions in attempts to capture key behavior of coupled process systems using the computational power available.

A thermal, hydraulic, mechanical or chemical process is described by a balance equation based on conservation of mass or energy. The key basic balance equations for the THMC processes are described below. Generally there will be one thermal process (T), one, two or in some cases three fluid flow processes (H) depending on how multi-phase flow is dealt with (see also Fig. 2.3), one mechanical process (M), and (n) chemical (C) processes included depending on the number of chemical species considered.

4.2.3 Thermal Process

For heat transport (T) the balance equation is given by Eq. (4.2.1).

$$D_T \Delta T - c^w \rho^w \nabla \cdot (qT) - \rho Q_T = c^m \rho^m \frac{\partial T}{\partial t} \tag{4.2.1}$$

where c^m is the specific heat of the saturated porous rock, c^w is the specific heat of the fluid, D_T is the heat diffusion dispersion tensor for the porous medium, T is temperature, ρ^w is fluid density, ρ^m is the density of the saturated porous rock, Q_T is a heat source or sink and q is the advective fluid velocity. Here, after de Marsily (1986), the heat diffusion dispersion tensor contains a component for pure diffusion and a component for dispersion due to advection, i.e.

$$D_\alpha = \lambda_m + q_\alpha \beta_\alpha \tag{4.2.2}$$

where β is the heat diffusion dispersion coefficient in the α direction, λ_m is the isotropic heat conductivity of the porous medium, q_α is the advective flow velocity in the α direction, and D_α is the heat dispersion coefficient in the α direction. The value β_α is the product of the directional (longitudinal or transverse) dispersion coefficient, with $c^w \rho^w$.

Equation (4.2.1) represents the change in the amount of energy in a continuum at a discrete location in a unit volume as a consequence of heat entering, leaving or being stored in the discrete unit volume either through conduction, radiation diffusion or convection.

4.2.4 Hydraulic Process

For single phase fluid flow (H), the hydraulic process is similarly described as being the change in the mass of fluid in a continuum at a discrete location as a consequence of fluid entering, leaving or being stored in the discrete unit volume either through advection, or addition/removal through a source term.

$$S_s \frac{\partial p}{\partial t} - \nabla \cdot \left(\frac{k}{\mu} (\nabla p + \rho g \nabla z) \right) = Q \tag{4.2.3}$$

where S_s is the specific storage coefficient, k denotes the permeability tensor, p is the fluid pressure, and Q is a source/sink term. This equation is valid for a saturated, non-deforming porous medium with heterogeneous hydraulic conductivity.

For multiphase flow including some solid deformation in the pore space

$$S_\alpha \rho_\alpha \nabla \cdot \frac{\partial \mathbf{u}}{\partial t} + \frac{\partial (\phi S_\alpha \rho_\alpha)}{\partial t} + \nabla \cdot (\rho_\alpha \mathbf{q}_\alpha) - \rho_\alpha Q_\alpha = 0 \tag{4.2.4}$$

The fluid velocity $\mathbf{q}_\alpha$ is a non-linear function of the pressure gradient, after Darcy's law as given above

$$\mathbf{q}_\alpha = \phi S_\alpha \mathbf{v}_\alpha = \frac{Q_\alpha}{A} = -\frac{k_{r\alpha} \mathbf{k}}{\mu_\alpha} (\text{grad}\, p_\alpha - \rho_\alpha \mathbf{g}) \tag{4.2.5}$$

where $k_{r\alpha} = f(S_\alpha)$ is discussed previously (Chap. 3). Here for the wetting phase

$$p_\alpha = p_w \tag{4.2.6}$$

and for the non-wetting phase, CO_2 in our example

$$p_\alpha = p_w + p_c \tag{4.2.7}$$

where p_c is expressed as a negative suction pressure.

4.2.5 Mechanical Processes

For mechanical processes (M), we again describe the deformation of a continuum as a function of the stress applied, which can be shown to be an energy balance equation. Again the basis for the analysis is that of the energy balance in a continuum at a discrete location as a consequence of stress and deformation changes within a discrete unit volume.

$$\nabla \cdot \sigma - \rho g = 0 \tag{4.2.8}$$

where σ is the stress, ρ is the medium density and g is the acceleration due to gravity.

4.2.6 Chemical Transport

Chemical transport (C) is described as being the change in the mass of a chemical species in a continuum at a discrete location as a consequence of fluid that species entering, leaving, being stored or being removed from the discrete unit volume either through advection, diffusion, sorption, or addition/ removal through reactivity, usually represented as a source term.

$$\frac{\partial C}{\partial t} = \nabla \cdot (D \nabla C) - q \cdot \nabla C + C_s \tag{4.2.9}$$

where C is the concentration, **D** is the dispersion tensor, q is the advective velocity, C_s is a concentration source/sink.

4.2.7 Solution of the Equation Systems

For each of the individual processes given above there are standard analytical solutions when considering the equation alone, e.g. Häfner et al. (1992), Bronstein and Semedjajew (1977). Coupling occurs when the solution of one process depends on the solution of another process. The link between the solutions of these processes is via the constitutive relationships, whereby the behavior of the material, fluid or energy is described mathematically as a function of the field variables of the processes involved in the solution. This makes the equations highly nonlinear.

Beyond a number of analytical solutions for idealized conditions, in heterogeneous systems the equations can either be solved in a staggered or non-staggered (monolithic) solution. A staggered solution involves the splitting of the system of equations into the individual processes. For each process the field variable is evaluated advanced with time, and the solution iterated internally between the split equations until a certain degree of accuracy in the solution is reached. Simplifications

of the solution procedure using explicit results can be useful, e.g. during creation of the elasto-plastic matrix during deformation, but must be applied with caution. For a non-staggered solution all the equations are combined into a single mass or energy balance formulation for solution and the whole problem is advanced simultaneously in time. In both cases strict time control is necessary and a number of numerical stability criteria need to be observed related to the geometrical discretization and the amount of energy or mass being moved around per time interval.

It can be pointed out that caution must be applied in overstating the need for mathematical accuracy in a geological systems given the parametrical uncertainty at several levels of the equation systems. Computationally expensive solution procedures valid for the aeronautical industry where the constitutional behavior and the parameterization of the material properties is known to within very tight limits may not be a priority when the constitutional behavior is dependent on the geology of the system and the uncertainty of material properties bound several orders of magnitude.

The processes will also vary in terms of their spatial impact and the rate of change of the field variable. For instance during CO_2 injection, the fluid pressure change may move rapidly through the porous media and impact a wide area, while the thermal change will be localized around the borehole, and chemical reactions associated with the injection of the CO_2 will be limited to the contact of the CO_2 being injected and the in situ reservoir fluids.

In terms of chemical changes, equilibrium solutions are often assumed in the multi-species simulations, basically because the complexity of the chemical system is at the limits of our reasonable computational possibilities. Given the possible thousands of interacting chemical species, key reactions need to be identified. These can be rate-limited but again there is much discussion regarding reaction rates and surface areas available to reaction. Unfortunately it appears that most lab based parameterization of reaction rates suggest much more rapid reaction of minerals than derived from natural analogues. The location of the growth or dissolution of minerals within the porous media can have a significant impact on the constitutive relationships such as the intrinsic permeability of the system, or the mechanical stability of the system. If a mineral grows in a fracture, the physical size of mineral growth filling or dissolving from the fracture is linked to the permeability by a cube of the fracture aperture. Modeling such systems can easily lead to a complexity not supported by available data, and at best an understanding of the impact of key material phenomena can be gained.

Likewise phenomena vary in terms of the spatial distance over which it occurs, as well as the rate of change. For instance during rapid advective flow of CO_2 through a fracture, the CO_2 will cover a large distance in the direction of the fracture whilst diffusion normal to the fracture into the rock matrix will be operating at a time scale orders of magnitude slower than the flow.

As would be expected, seeking for efficient solutions of highly nonlinear partial differential equations has been of great scientific interest since the beginning of the last century. Numerous publications and journals are dedicated to this theme. There exist already a number of industrial and research codes developed and tested for the

solution of the coupled processes. Prominent examples include the developments of the (1) TOUGH2 family of codes, including TOUGHREACT (Xu et al. 2014) for solving coupled hydro-chemical processes in multiphase CO_2 storage scenarios and TOUGH-FLAC (Rutqvist 2011) for hydro-mechanically coupled systems (http://esd.lbl.gov/research/projects/tough); (2) Open GeoSys (http://www.opengeosys.org) (Kolditz et al. 2012a) and Code Bright (http://www.etcg.upc.edu/recerca/webs/code_bright) (Olivella et al. 1996). These codes require expert users able to clearly define the systems they are attempting to model and with an understanding of which phenomena to include and exclude. There is no "off the shelf" solution for the selection of the codes which can be used. Several international collaboration projects have been looking at different numerical code possibilities and benchmarking their success to improve confidence of use. Examples include http://www.cgseurope.net/ and the IEAGHG modeling network.

In Sect. 4.4 we will present some example applications of coupled modeling with these models, addressing the coupled hydro-chemical (HC) system and the coupled hydro-mechanical (HM) system.

4.3 Modeling of the Small Scale Effects

Henry Power, Jesus Carrera and Christian Ian McDermott

In this section modeling of two important small-scale processes related to geological storage of CO_2 are discussed, namely the processes of convective dissolution and viscous fingering.

4.3.1 Convective Dissolution

Jesus Carrera

CO_2 injection in saline aquifers leads to a CO_2 plume that is less dense than the brine and floats on it while spreading horizontally. CO_2 solubility is quite high, so that a significant portion of CO_2 dissolves into the brine at the interface between the two fluids. CO_2 dissolution is favourable for several reasons. First, by reducing the volume and pressure of the free phase, dissolution reduces the risk of CO_2 phase leaking upwards. In fact, migration of dissolved CO_2 is hard both because the viscosity of brine is much larger than that of any CO_2 phase and because CO_2–rich brine is 1–2 % denser than resident brine, so that it will tend to sink. Second, dissolution facilitates that CO_2 transforms to more stable species such as bicarbonate or, if geological conditions are favourable, mineral carbonates.

CO_2 dissolution into the brine is initially controlled by diffusion from the CO_2-brine interface, which is a slow process with mass flux evolving proportional to $t^{-1/2}$, t being time. For this reason, early estimates of dissolution were quite pessimistic, predicting it would take some 1000 years for dissolution to be a relevant process (IPCC 2005). However, as the amount of dissolved CO_2 builds up, the resulting conditions (denser liquid on top) are unstable, so that the CO_2 rich brine will tend to sink, thus promoting the convective transport of dissolved CO_2 away from the CO_2 phase plume. In fact, Riaz et al. (2006) showed that this mechanism can reduce significantly the dissolution time.

The question is how long it takes for the instability to develop. Riaz et al. (2006) found that the onset of instability may take some 100 years. However, they made a number of simplifications that may be critical. The first one is the analogy to a heat transport problem. This is a common simplification, because of the tradition of studying convective transport of heat. In a heat transport model, fluid may be assumed to consist of a single component. As such, heat transport and fluid flow are basically linked through the buoyancy term. However, in mass transport problems the fluid must be viewed as consisting of at least two components (i.e. brine and CO_2). Since the flow equation expresses the mass balance of the whole fluid phase, additions of any of the two components must be accounted for in it. Specifically, while an impervious boundary (i.e. a boundary with zero brine flux) can be treated as a zero mass flux in thermal problems, it must allow for fluid mass flux (CO_2 component) in mass transport problems (Hidalgo et al. 2009b). The second issue refers to the simplifications assumed for flow and transport problems. For flow, fluid is considered incompressible and the Boussinesq approximation valid. However, acknowledging compressibility of the fluid helps in simulating the pressure rise caused by the influx of CO_2, which helps promoting CO_2 flux downwards. Boussinesq approximation may affect the transient solution (Johannsen 2003a), although it is valid for the typical range of values of the Rayleigh number (see Landman and Schotting 2007). For transport, dispersion is neglected. Hydrodynamic dispersion accounts for the effects of the deviations from the mean flow caused by small scale heterogeneity on solute transport. Heterogeneity is present in all natural systems; therefore, dispersion has to be included in any realistic transport formulation. Notice that in thermal analogies, which are the base of many CO_2 dissolution models, dispersion is often neglected. This is arguably done (See, e.g., Ferguson and Woodbury 2005; Hidalgo et al. 2009a) because of the relatively large value of thermal conductivity. However, dispersion cannot be disregarded in solute transport because it can be much larger than molecular diffusion. In fact, dispersion can be artificially increased if a fluctuating injection regime is adopted (Dentz and Carrera 2003).

In the following, we summarize the work of Hidalgo et al. (2009a) on how a more realistic representation of CO_2 dissolution affects the time for the onset of convection and the estimation of the CO_2 flux across the interface.

4.3.1.1 Governing Equations

The compressible density-dependent flow and advective–diffusive–dispersive transport equations that govern the CO_2 dissolution in a saline aquifer are written as (recall Chap. 3):

$$\rho S_p \frac{\partial p}{\partial t} + \rho\theta\beta_\omega \frac{\partial \omega}{\partial t} = -\nabla \cdot (\rho \mathbf{u}) \tag{4.3.1}$$

$$\rho\theta \frac{\partial \omega}{\partial t} = -\rho \mathbf{u} \cdot \nabla\omega + \nabla \cdot (\rho(\theta D_m + \mathbf{D})\nabla\omega) \tag{4.3.2}$$

where ρ is fluid density, S_p the specific pressure storativity ($S_p = S_s\rho_{wg}$, where S_s is the traditional specific storativity), p pressure, θ the volumetric fluid content, $\beta_\omega = (1/\rho)\partial\rho/\partial\omega$ expresses the brine density dependence on CO_2 mass fraction, considered constant, ω the CO_2 mass fraction, $\mathbf{u}$ the Darcy velocity and $\mathbf{D}$ the hydrodynamic dispersion tensor, as described in Chap. 3.

The dissolution interface between the CO_2 and the brine is located to be at the top of the domain, i.e. z = 0, and it is modeled as a prescribed concentration boundary. The domain is conceptually considered semi-infinite, i.e. there is no interaction with the lower and lateral boundaries. Therefore, boundary conditions are written as:

$$\begin{array}{cc} -\rho\mathbf{u}|_b \cdot \mathbf{n} = m_s & \text{if } z = 0, \\ \rho\mathbf{u}|_b \cdot \mathbf{n} = 0 & x, z \to \infty, \end{array} \tag{4.3.3}$$

for flow and

$$\begin{array}{rcll} \omega|_b & = & \omega_s & \text{if } z = 0, \\ (-\rho\mathbf{u}\omega + \rho(\theta D_m + \mathbf{D})\nabla\omega)|_b \cdot \mathbf{n} & = & 0 & x, z \to \infty, \end{array} \tag{4.3.4}$$

for transport. In these equations $\mathbf{n}$ is the unit vector normal to the boundary pointing outwards, $m_s[ML^{-2}T^{-1}]$ is the CO_2 mass flux across the top boundary, ω_s is CO_2 solubility in brine (highly sensitive to both pressure and salinity, see Sect. 3.2) and $|_b$ indicates evaluation at the boundary.

The conceptual model proposed by Eqs. (4.3.1)–(4.3.4) introduces significant modifications with respect to previous CO_2 dissolution models. First, governing equations acknowledge fluid compressibility and hydrodynamic dispersion. Second, boundary conditions include the CO_2 mass flux across the top boundary. This CO_2 flux is

$$m_s = (-\rho\mathbf{u}\omega + \rho(\theta D_m + \mathbf{D})\nabla\omega)|_b \cdot \mathbf{n}. \tag{4.3.5}$$

Subtracting (4.3.3) multiplied by ω from (4.3.5) yields

$$m_s = \frac{1}{1-\omega}\rho(\theta D_m + D_{zz})\frac{\partial \omega}{\partial z}, \tag{4.3.6}$$

where it has been imposed that the concentration gradient is vertical.

For analysis purposes, it is convenient to write governing equations in a dimensionless form. We adopt the characteristic space and time, respectively, as

$$L_s = \frac{\theta D_m + \alpha_L u_b}{u_b}, \qquad t_s = \frac{\theta(\theta D_m + \alpha_L u_b)}{u_b^2} \tag{4.3.7}$$

where $u_b = k\Delta\rho g/\mu$ is the modulus of velocity when CO_2 is dissolved at saturation ($\omega = \omega_s$), and $\Delta\rho$ is the density contrast between the brine and the CO_2-saturated brine (see Sect. 4.2 for values of both densities). This choice leads naturally to the following dimensionless variables (prime denotes dimensionless variable): $p' = pS_p/\theta$, $\rho' = \rho/\Delta\rho$, $\mathbf{u}' = \mathbf{u}/u_b$, $(x', z') = (x, z)/L_s$ and $t' = tu_b/\theta L_s$.

Using these scaling factors, the dimensionless form of flow and transport equations becomes

$$\frac{\partial p'}{\partial t'} + \frac{\partial \omega'}{\partial t'} = -\frac{1}{\rho'}\nabla' \cdot (\rho' \mathbf{u}') \tag{4.3.8}$$

$$\frac{\partial \omega'}{\partial t'} = -\mathbf{u}' \cdot \nabla'\omega' + \frac{1}{\rho'}\nabla' \cdot (\rho'((1-b_L)\mathbf{I} + b_L\mathbf{D}')\nabla'\omega'), \tag{4.3.9}$$

where b_L is defined as

$$b_L = \frac{\alpha_L}{L_s} \tag{4.3.10}$$

with the corresponding dimensionless boundary conditions. Notice that, because we are using a semi-infinite domain, we do not use a Raleigh number. Still, for comparison purposes, we define it as $R_a = u_b L_s/\theta D_m$, where D_m is the molecular diffusion coefficient.

4.3.1.2 Numerical Analysis

CO_2 dissolution was simulated using the code Transdens (Hidalgo et al. 2005). Transdens solves density-dependent flow and transport problems using a finite element discretization in space and weighted finite difference in time. Reverse time weighting by Saaltink et al. (2004) is used to minimize mass balance error during time integration. Darcy velocity is computed using the consistent velocity algorithm by Knabner and Frolkovic (1996). The code was validated using the usual density-dependent problems benchmarks and by comparison with other codes.

Instabilities in the system were not seeded explicitly, but by the propagation of numerical errors. Simulations were carried out on a squared domain of 10 × 10 m (dimensionless size between 17.86 and 2000 depending on b_L), which proved to be large enough to warrant that there was no interaction with the lower boundary. The domain was discretized with a mesh of rectangular finite elements of 101 × 201 nodes. For comparison purposes, parameters were chosen equal to those of Riaz et al. (2006) (H = 10 m, $k = 3.0581 \times 10^{-13}$ m^2, $\theta = 0.3$, $D = 10^{-9}$ m^2/s, $\mu = 5 \times 10^{-4}$ Pa s, $\Delta\rho$ kg/m^3), details are shown by Hidalgo and Carrera (2009).

Our findings are summarized in Figs. 4.4, 4.5 and 4.6. Figure 4.4 displays the growth of fingers. Figure 4.5 displays the time evolution of CO_2 mass flux. Dissolution is initially controlled by diffusion. Therefore, it decays as $t^{-1/2}$. However, when fingering develops, the dimensionless mass flux fluctuates around 35 ω_s, which is indeed a very simple expression. Notice that it is not sensitive to dispersion, but basically to permeability and buoyancy forces. Figure 4.6 displays the onset time of convective dissolution. Again a simple expression t_{onset} = 5619–5731b_L fits data quite well.

The topic has been extensively studied since Riaz et al. (2006) and Hidalgo et al. (2009a). High resolution simulations were performed by Pau et al. (2010), the effect of geochemistry and reactive transport was studied by Ghesmat et al. (2011), Hidalgo et al. (2015), and Fu et al. (2015); the effect of the capillary transition zone was studied by Elenius et al. (2014) and Emami-Meybodi and Hassanzadeh (2015). Visualization experiments have been performed after Neufeld et al. (2010) and MacMinn et al. (2011). Rasmusson et al. (2015) studied the prerequisites for convective mixing for a wide range of field conditions.

The summary of all this work is that the phenomenon is complex. Szulczewski et al. (2013) identify seven dissolution regimes. But, for most practical purposes, three sequential regimes are dominant:

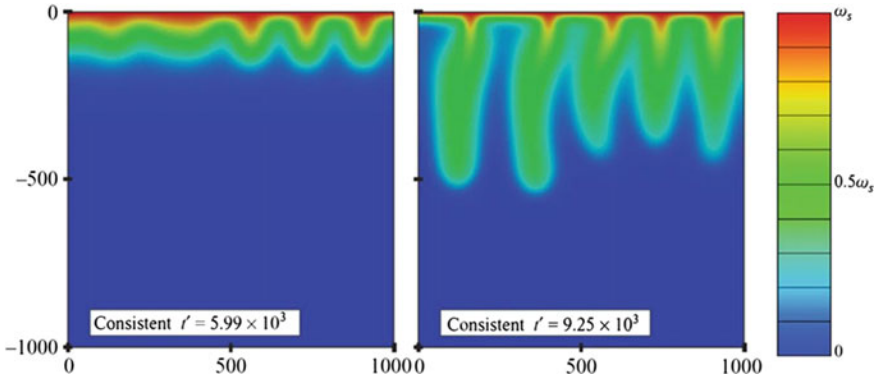

Fig. 4.4 Onset of fingering

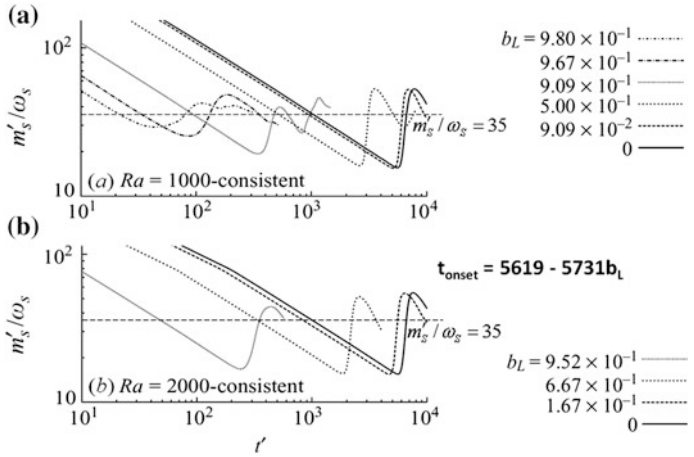

Fig. 4.5 Time evolution of the CO_2 mass flux (dimension rate) for Rayleigh number of **a** 1000 and **b** 2000. The CO_2 dissolution flux is initially controlled by diffusion (dispersion) but increases to values that fluctuate around $m_s' = 35\omega_s$ after the onset of fingering. While the onset time depends on dispersion (b_L), the mass flux does not

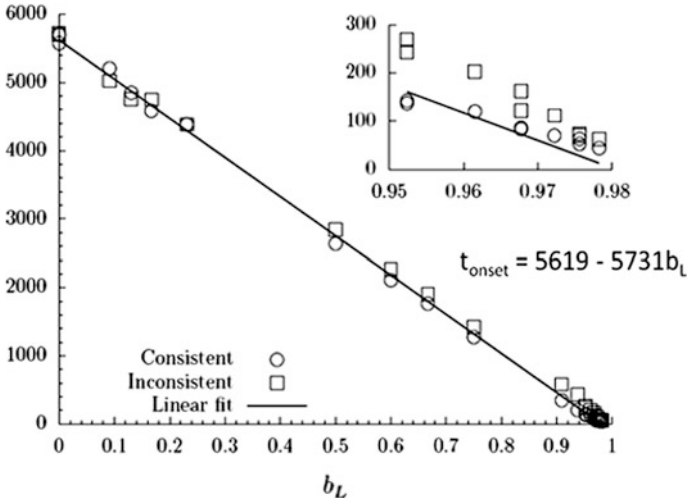

Fig. 4.6 Dimensionless time for the offset of convection versus dimensionless dispersion (Hidalgo and Carrera 2009). Notice that dispersion brings a dramatic decrease in the time for the onset of convection

1. *Diffusive Regime* Dissolution is controlled by diffusion away from the CO_2 plume until the onset of fingering. The time for this onset is greatly reduced by dispersion, which is important because dispersion can be increased by simply adopting a fluctuating injection regime. It is also reduced by capillarity. In fact,

visualization experiments suggest that it is virtually simultaneous with the development of the plume.
2. *Convective Dissolution* The mass flux after fingering develops is constant (except for capillarity effects) and virtually insensitive to dispersion. It solely depends on permeability and buoyancy and equals $m = \alpha\omega_s\rho u_b$, where α was evaluated as 0.0142 in the work of Hidalgo and Carrera (2009), but is usually taken as 0.0175, resulting from the high resolution simulations of Pau et al. (2010).
3. *Shutdown Regime* As concentration below the interface starts increasing, the density difference drops and so does u_b. This can be assumed to occur when the fingers reach the aquifer bottom. After this time, dissolution is approximately proportional to the difference between the average concentration in the brine and the saturation concentration, ω_s.

4.3.2 Viscous Fingering

Christopher Ian McDermott and Henry Power

In this section we will consider the interfacial instability between two immiscible fluids in a porous media, during the displacement of brine (wetting fluid) by an injected supercritical CO_2 (non-wetting fluid). Supercritical CO_2 has a lower density and viscosity than the surrounding brine. Therefore, at moderate capillary number, as the plume of the injected CO_2 evolves, the interface between the two fluids will develop viscous fingering patterns. Besides, the supercritical CO_2 in contact with the brine dissolves into the liquid phase, having a large contact surface area due to the fingering structure of CO_2–brine interface.

Viscous fingering instability of immiscible fluids displacement in porous media can be studied by numerical simulation of the multiphase flows formulation, in terms of the saturation index S_w where a flow region of overlapping between the fluids is considered for $0 \leq S_w \leq 1$ without a specific definition of the fluid interface. This type of approach has been reported in the literature by several authors, including Huang et al. (1984), Yortsos and Huang (1984) and more recently Garcia and Pruess (2003) and Riaz et al. (2006). By use of this type of formulation, however, direct implementation of interfacial processes is not possible. Several numerical techniques have been proposed in the literature to include the existence of an interface, with the objective of incorporating some of the interfacial processes in the formulation [for more details see McDermott et al. (2011)]. In the next section we will discuss different approaches of front tracking for multiphase flow and present an illustrative example of application of one of the methods.

4.3.2.1 Front Tracking Numerical Algorithms for Multiphase Flow Simulations of Viscous Fingering

Modeling two-phase flow using standard grid based numerical techniques presents a problem due to the sharpness of the front developed by the replacement of one fluid with another, balanced against the need to discretize the model into grid points and elements. One of the issues is that changes due to coupling to other processes, such as mechanical faulting and pressure release of the fluid, is likely to occur as the front passes. Depending on the resolution of the fluid flow grid, this time dependent signal may be missed or smeared with other signals loosing information on the integrity of the reservoir. In finite element approaches lower order based interpolation functions often fail to represent the sharp front and this can also lead to oscillations around the true solution. Finite volume methods can avoid these oscillations, but there are issues concerning the relative computational expense of these formulations and difficulties in representing smoothly varying heterogeneity fields while minimizing discretization overheads. Mixed finite element solutions whereby both the velocity field and the pressure solution are considered primary variables are finding some acceptance; however they are computationally more complicated to implement, especially with respect to solver capabilities (Younes et al. 2010).

Three main approaches have been adopted to address this problem. The most widely adopted approach is that of **grid refinement,** or adaptive mesh refinement in the vicinity of the front. The geometry of the grid is locally adapted to better represent the numerical processes operating at a local scale and represent steep gradients within the model. Recent examples for highly heterogeneous fields include Chen et al. (2003) and Durlofsky et al. (2007). Such adaptive grid methods allow the discretization scale to follow the front through the model, however the front location will always be approximated within the scale of the discretization used. Such methods are extremely useful but can be computationally expensive and make coupling to other processes such as thermal, mechanical, reactive chemical (TMC) more complicated due to the constant alteration in grid size and location.

Interface tracking methods have been developed that apply sophisticated reconstruction algorithms based on either the ratio of volumes of a fluid in an element (volume of fluid methods) or the advective velocity of the interface throughout the modeling regime (level set method). Meakin and Tartakovsky (2009), with references therein, review these approaches and conclude that there has actually been very little application of these techniques to multiphase fluid flow in fractured and porous media. Recent examples of their application include Huang and Meakin (2008), Huang et al. (2005) and Unverdi and Tryggvason (1992). Glimm et al. (1999) tracked the front throughout the computational domain using a grid based interface reconstruction based on information in the grid element and the information from surrounding elements. Interface tracking methods address the problem of the location of the front based on the volumetric fluid fluxes into and out of an element, the understanding that there must be continuity between elements and assumptions as to the shape of the front.

McDermott et al. (2011) in turn presented an alternative development of a front tracking based on a **local one-dimensional analytical approximation** of the fluid interface to add information to the model and to predict the location and shape of the front within the elements. The assumption removes the necessity for adaptive mesh refinement and the need for further sophisticated reconstruction of the front surface. The information on the geometry of the front surface under the conditions given in the element is being predicted by the locally one-dimensional representation of the front. The method increases the accuracy of the prediction of the front location, but is still bound by the overall accuracy of the numerical method applied to determine the primary variables which the analytical solution depends upon.

In the approach, the standard two-phase flow equations described in Chap. 3 are solved using the IMPES (implicit pressure explicit saturation) formulation (e.g. Helmig 1997). The saturation equation is formulated in terms of the volume of replacing fluid in the discretised elements. This volume may either be predicted using a standard first order approximation, or by using the analytical solution of the location of the front directly and integrating under this front. The latter approach works for homogenous conditions, and predicts radial flow better than the standard numerical methods using full up-winding schemes, however, still requires further development for heterogeneous conditions.

The unknowns of the wetting phase pressure and the non-wetting phase saturation are solved sequentially using different approaches. For the pressure formulation the Full upwind galerkin (FUG) finite element method is used, providing maximum mobility and for the solution of the saturation equation we introduce extra information in the model by including an analytical derivation of the shape function for the evaluation of the saturation front. The details of the approach and the numerical implementation are given in McDermott et al. (2011) and are not repeated here.

The advantage of using an analytical derivation for the location of the saturation front is that it removes the necessity to refine the mesh in the locality of the saturation front whilst still maintaining the sharpness of the front without numerical oscillations. The method, however, still has the requirement that the Courant time criteria apply for the advective flux of the front (Kolditz 2001), and, as is the case using a FUG scheme, numerical diffusion is introduced. In addition, the accuracy of the location of the front prediction is dependent on the accuracy of the numerical solution of the primary variables.

To demonstrate the use of this hybrid method for the solution of two phase flow and the prediction of the front, we assume simplistic conditions. First it is assumed that there is no pressure difference across the liquid–liquid phase boundary, i.e. capillary pressure effects are negligible. The second assumption is that the solid–liquid–liquid contact angles have no significant impact on the flow characteristics. This approximation means that the capillary pressure term P_c is neglected in the pressure formulation. It needs to be pointed out that at the pore scale it would be necessary to include these effects, as discussed in detail by Meakin and Tartakovsky (2009) and references therein. Niessner and Hassanizadeh (2008) in turn examine the role of fluid–fluid interfaces and the impact they can have, such as hysteresis. At

the macroscopic scale, given the heterogeneity of geological medium and the assumption of generally continuous fluid phases, these simplifications can, however, be considered valid.

For the demonstration example presented in detail in McDermott et al. (2011) we assume constant density and no deformation. To be able to evaluate the volume of the replacing fluid, the volume underneath the saturation surface needs to be calculated. Different analytical approximations can be considered for determining the location of the two phase flow front. Here for the demonstration of the method we apply the original 1D analytical solution derived by Buckley and Leverett (1941) for the replacement of one fluid with another in two phase flow.

The *Buckley* and *Leverett* solution is one of the simplest for two phase flow where capillary pressures are not considered to be causing any resistance to flow. The capillary pressure is, however, included indirectly in terms of allowing residual trapping by the consideration of a residual saturation for the calculation of the relative permeability functions below. Buckley and Leverett (1941) used relative permeabilities described by the functions given below (4.3.11) derived from their laboratory work.

$$k_{r1} = \frac{(S_1 - S_{1r})^2}{(1 - S_{1r} - S_{1r})^2} \quad \text{and} \quad k_{r2} = \frac{(1 - S_1 - S_{2r})^2}{(1 - S_{1r} - S_{2r})^2} \tag{4.3.11}$$

The *Buckley* and *Leverett* analytical solution of the saturation equation considering fractional flow functions is presented by Thorenz et al. (2002) as being

$$\Delta x = -\frac{u_{total}}{\phi} \frac{\partial \left(\frac{1}{1 + \frac{k_{r2}\mu_1}{\mu_2 k_{r1}}} \right)}{\partial S} \Delta t \tag{4.3.12}$$

From this equation it is possible to derive the saturation curve presented in Fig. (4.7a). The Eq. (4.3.12) has two possible saturations for one location. Using the equal area solution the actual location of the saturation front is determined by constructing a shock front whereby "Area 1" is equal to "Area 2" (see Fig. 4.7b).

In Fig. (4.7), the solution of the *Buckley and Leverett* equation has been normalised against the maximum distance *md* from the origin for the extension of the saturation front. Examining (4.3.12) it can be seen that the term $\frac{u_{total}}{\phi} \Delta t$ is a scaling term, and for the solution presented in Fig. (4.7) we set this to 1.

This means that it is possible for any combination of flow rates, porosity and time to be compared with the normalized analytical solution via a scaling factor. This fact is central to the application of this analytical solution.

The shape of the analytical solution from the origin to the saturation front can be approximated by a polynomial fitted to match the normalized analytical response (Fig. 4.7b). Therefore a standard response for the solution assuming constant

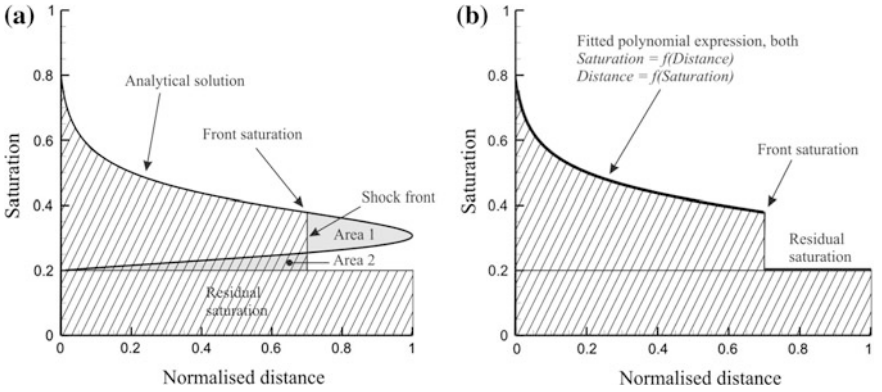

Fig. 4.7 **a** One-dimensional analytical solution for two phase flow and **b** the two-phase flow surface is approximated by a polynomial expression (McDermott et al. 2011)

material permeabilities and viscosities within an element may be evaluated by solving (4.3.12) and applying the appropriate scaling term. Depending on the saturation values of the nodes, the saturation front may be (1) present within the element, (2) have passed through the element, (3) not have reached the element. Each of these cases is handled individually and more details can be found in McDermott et al. (2011). For a detailed description of the comparison between the simplified 1D analytical solution for two phase flow by Buckley and Leverett (1941), and the different the FUG schemes see McDermott et al. (2011).

4.3.2.2 Demonstrative Example: Well Injection in a Heterogeneous Reservoir Rock

The proposed approach by McDermott et al. (2011) is used to simulate injection of supercritical CO_2 into a reservoir layer underlying a caprock. The fluid and material properties are also given in the above reference and are not repeated here.

The CO_2 spreads out laterally from the injection point, and forms channels as a result of the heterogeneity. This is demonstrated in Fig. 4.8, left, where the front tracking method can be seen to be providing sub-element scale information on the location of the saturation front. In Fig. 4.8 we also compare the results of a finite volume approach utilizing an identical physical model and the method presented by McDermott et al. (2011), the latter with and without front tracking. In this figure the front tracking location is presented, then removed for comparison to the finite volume (FV) approach. We note that the overall shape of the predicted radial flow patterns is similar, and many features can be cross referenced. The FUG-vT method predicts the formation of more discrete and higher saturated channels, while the Finite Volume scheme predicts more distribution in the saturating phase. This is due

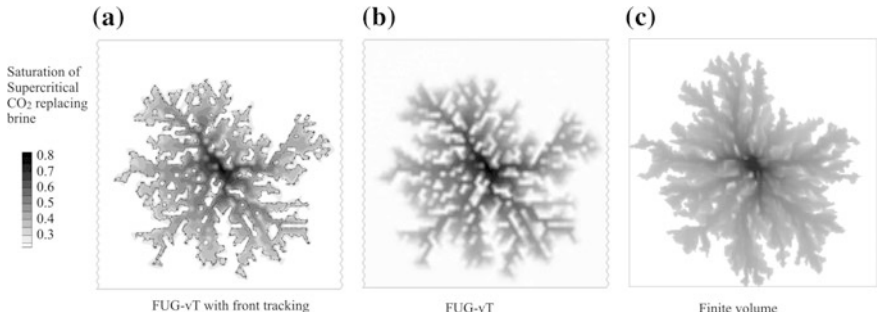

Fig. 4.8 Comparison of well injection of supercritical CO_2 in a heterogeneous reservoir rock. **a** FUG with front tracking, **b** FUG without front tracking and **c** a finite volume solution (McDermott et al. 2011)

in part to the differences in the numerical schemes, specifically concerning the tendency for the finite element approach to 'blur' permeability contrasts across elements as the fluxes are assigned to the nodes by integrating across the elements. This creates the possibility for channelled pathways that the finite volume approach would not include.

Strictly speaking the proposed model does not allow capillary trapping to occur, although the pattern of flow predicted would suggest this. The flow in the system is driven by the source term representing the well and pressure field developed by the well. Preferential flow as a consequence of the heterogeneous permeability field leads to the partial isolation of low permeability blocks within the flow system. This is exaggerated by the positive feedback caused by the relative permeability functions, i.e. the higher the saturation, the higher the permeability. Should capillary pressure also be included in the calculation, these low permeability areas would be even more sealed from the preferential flow channels. For more details of the practical application of the proposed mixed approach, advantages and disadvantages, see McDermott et al. (2011).

4.3.2.3 Effect of Dissolution on the Evolution of Viscous Fingering

Chuoke et al. (1959) pioneering work provides a theoretical analysis of the onset of viscous fingering in immiscible displacements in porous media by using the similarity between Hele-Shaw and porous media flows and ignoring the zone of partial saturation or volume concentration of the displacing fluid behind the front (capillary trapping) . In this type of approach, the existence of a sharp interface between the immiscible fluids is considered, corresponding to a macro average (representative elementary volume REV) of the interface at the micro-level between the immiscible fluids, in contrast with a volume of fluid formulation described in terms of

saturation index (multiphase flow formulation), where a flow region of overlapping fluids is considering for $0 \leq S_w \leq 1$ without a specific defined definition of a fluid interface.

Sharp interface approach requires the definition of different equations of motion on each side of the interface and the tracking of the interface motion as the flow progresses, allowing direct consideration of interfacial processes by including them into the corresponding matching condition at the interface. In the case of a two dimensional immiscible displacement in a porous medium, fingers of width given by the characteristic scale $w \sim \left(\frac{k}{N_{Ca}}\right)^{1/2}$ found by the Hele–Shaw approximation, under-predict the experimental observations. This has led to the hypothesis of an effective surface tension γ , larger than the molecular surface tension and function of the wetting conditions, that varies with the large-scale curvature at the macro-scale (see Weitz et al. 1987). The use of a modified jump condition in terms of the effective surface tension is known as Chouke's boundary condition and the resulting interface instability analysis is referred to as Hele–Shaw–Chouke theory (for more details see Homsy 1987). As commented by Homsy, it is not clear how surface tension acting at the menisci in the pore space can provide a restoring force proportional to the macroscopic curvature. However, strong experimental evidence has been reported in the literature with excellent agreement between the experimentally observed characteristic macroscopic length scales and Hele–Shaw–Chouke predictions, by fitting the value of the effective surface tension. Most of the works dealing with immiscible displacement have been focused on two-dimensional cases. However, some works have also addressed the difference between two- and three-dimensional displacements (Xiaoping et al. 1997).

In the multiphase flow approach presented in the previous section, the variations in saturation in the overlapping region result in a gradual change of the mobility of both phases. This type of analysis is closely related to the stability of graded mobility process, see Gorell and Homsy (1983) and Hickernell and Yortsos (1986), where depending upon the mobility function a displacement that has an unfavourable viscosity ratio may still be linearly stable, even at infinite capillary number. Homsy's (1987), review article presents a very detailed analysis of these two types of approach, i.e. sharp front (Hele–Shaw–Chouke) and saturation index (multiphase flow). Besides, in the article he addresses the similarity between changes of mobility due to variation in saturation during immiscible displacements and due to changes in concentrations in miscible displacements.

In the sharp interface approach, the effect of capillary trapping of the wetting fluid (brine) on the evolution of CO_2 plume (non-wetting fluid) is not considered, which results in a local reduction of the difference between the mobility of the two phases and consequently affects the fingering evolution. Daripa and Pasa (2008) presented an analysis showing that the slowdown of instabilities due to capillarity is usually very rapid which makes the flow almost, but not entirely, stable. New sharp interface formulations and numerical solutions explicit consider the effect of dynamic wetting by including a nonlinear term in the pressure jump condition due

to the trailing film left behind by the displaced fluid. Jackson et al. (2015a) used this type of approach to study the effect of capillary trapping on the nonlinear evolution of radial viscous fingering in a Hele–Shaw cell and observed that finger interaction is reduced and finger breaking mechanisms delayed but never fully inhibited, which allows the primary fingers to advance further into the domain before secondary fingers are generated, reducing the level of competition.

In this section we will present an analysis of the coupling effect between the surface dissolution at the interface between two immiscible fluids and the evolution of viscous fingering in a Hele–Shaw cell (for more details see Power et al. 2013). Dissolution processes will change the kinematic and dynamic conditions at the fluid interface of an immiscible displacement and consequently the dynamics of any interfacial instability. For simplicity in the present numerical solution a single-phase approximation is considered, this implies that the viscosity of the less viscous fluid is so small that it may be ignored. In the case of CO_2 sequestration, the viscosity of the CO_2 gas can be one or two orders of magnitude smaller than the brine's viscosity. Therefore, the type of single-phase formulation presented here only provides a leading order approximation of the complete asymptotic regular perturbation approach in terms of the viscosity ratio of the problem. The reader is referred to Jackson et al. (2015b) for an extension to a two phase formulation of the single phase approach presented here, where direct account of the viscos effects of the injected CO_2 and resident brine is considered.

The mathematical modeling of viscous fingering in Hele–Shaw cell is generally carried out by using a potential model formulation. Hele-Shaw flow takes place when a viscous fluid moves slowly between two fixed parallel plates, separated by a thin gap. The mean flow is two-dimensional, and the mean velocity components in the plane of the cell are related to the mean pressure by Darcy equations $u_i = -M\partial p/\partial x_i$ with $M = b^2/12\mu$ which is a function of the plate gap b and the fluid viscosity μ. For incompressible fluid of constant viscosity the conservation of mass implies that $\partial^2 p/\partial x_i^2 = 0$, i.e. the Laplace equation.

The boundary conditions at infinity are those for a growing bubble, i.e. constant pressure, while the boundary conditions at the fluid interface Γ are given by the kinematic and dynamic conditions obtained from the conservation of mass and momentum across the interface. In the evolution of the moving front, the patterns of the interfacial fingering are determined by the interface kinematic and dynamic matching condition. In the present case, the transfer velocity of the dissolved gas reduces the interface displacement velocity described by the kinematic matching condition, delaying the evolution of the fingering. On the other hand, the momentum flux across the interface, due to the CO_2 dissolution, modifies the dynamic matching condition at the interface with possible changes in the fingering pattern.

The interface matching conditions are obtained by considering the surface separating the two-phase flow (in reality the two flows are separated by a complex, narrow transitional layer, which is modeled here as a simple surface, see Edwards et al. 1991), which is represented here as a material pillbox straddling the moving

and deforming interface between the two-phases, as shown in Fig. 4.9, where the pillbox encloses a small fluid volume in contact with the interface having an internal surface S and an interface surface E. At the pillbox, mass and momentum conservation are imposed and the corresponding kinematic and dynamic interface matching condition obtained by taking the limit when the surface S tends to the interface surface E (see Power at el. (2013) for more details). In contrast to cases without gas dissolution into the brine, where, as the interface develops fluid does not cross the interface, in the present case, CO_2 crosses the interface by dissolution to become part of the brine liquid. Under this condition, the sharp interface is represented as a moving driving surface, i.e. a surface at which density and velocity are discontinuous and mass and momentum are transferred across it (see Slattery 1999). In our case, the mass and momentum transfer is associated with the interface due to the dissolution process.

The detailed derivation of the approach is given in Power et al. (2013) and will not be repeated here. Where due to the dissolution of the CO_2 into the brine at the interface, two new terms are included in the interface matching condition; a mass transfer term, $\rho_g u_d$, in the kinematic condition and a momentum transfer, $\rho_g u_d^2$, in the dynamic condition with u_d being the dissolution rate velocity.

As previously commented in Sect. 4.3.1, at the fluid interface CO_2 will dissolve into the aqueous phase, where by the difference in density of the developed fluid mixture and the local brine a convective flow is induced, promoting gravitational instabilities and the formation of density fingering. According to the conservation of mass, the descending mixed fluid along the fingers will induce recirculation cells of brine fluid between the fingers with an associated fluid entrainment into the fingers from the surrounding brine. The entrained brine reduces the density difference and the CO_2 concentration at the interface diffusive boundary layer, resulting in enhancement of the dissolution process (convectively-enhanced dissolution) . Recent experimental and numerical studies by Kneafsey and Pruess (2009) and Neufeld et al. (2010) (see Sect. 4.3.1) have observed that the convectively-enhanced dissolution process tends to produce an almost constant dissolution flux after only a very short time, which will persist for a very long time, i.e. on the scale of years, corresponding to the constant values in Fig. 4.5, i.e. the horizontal lines in the figure for each Rayleigh number. Ward et al. (2014a, b), studied the effect of

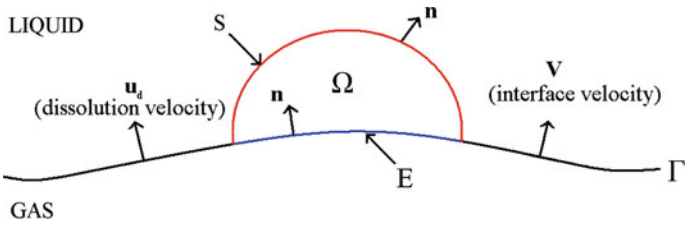

Fig. 4.9 Definition of pillbox at the fluid interface

chemical reactions on the convective enhanced dissolution process by considering that the solute concentration decays via a first-order chemical reaction, restricting the depth over which solute can penetrate the domain. Their simulations and analysis suggest that the time-averaged CO_2 uptake rate (dissolution flux) follows the classical scaling, namely being proportional to Ra (Rayleigh number), as observed in Fig. 4.5. However, the dissolution flux has a strong dependence on Ra. This provides evidence that the flux is restricted by the boundary layer, and that the plumes beneath accommodate this constraint. For convenience in this work, we will consider the CO_2 dissolution velocity to have a constant value, found from the dissolution flux estimates of Kneafsey and Pruess (2009) and Neufeld et al. (2010).

4.3.2.4 B-Spline Boundary Element Formulation (BEM) and Numerical Scheme

Since the interface between the two fluids experiences large deformations, and the correct determination of its shape is of foremost importance, the use of boundary integral representation (potential theory) is an attractive approach to find the numerical solution of the problem that has been successfully implemented before, see Degregoria and Schwartz (1986), Tosaka and Sugino (1994), Power (1994) and Zhao et al. (1995). On the other hand, in an immiscible displacement, surface tension plays a dominant role in the evolution of the viscous fingers, and so it is important that the shape of this interface is properly modeled in order that the local curvature at each interface point may be accurately evaluated. For this reason Power et al. (2013) employed boundary element formulation (BEM) model employing uniform cubic B-splines both for the geometry and the field variables is implemented, following Cabral et al. (1990) and Zhao et al. (1995).

In Power et al. (2013), the pressure field is expressed as a source potential (injection flux) plus a bounded perturbed field.

$$p = \hat{p} + \frac{Q}{2\pi M} \ln\left(\frac{r}{r_a}\right) \tag{4.3.13}$$

Therefore a boundary integral representational formula for the perturbed pressure evaluated at the fluid interface can be written in terms of the Laplace fundamental solution and corresponding flux, as (see Power and Wrobel 1995):

$$c(\xi)\hat{p}(\xi) = \int_{\Gamma} \hat{p}(\chi) q^*(\xi, \chi) d\Gamma_\chi - \int_{\Gamma} \hat{q}(\chi) p^*(\xi, \chi) d\Gamma_\chi + p_c, \tag{4.3.14}$$

where $c(\xi) = \theta/2\pi$, θ is the internal angle subtended at the source point ξ, $p^*(\xi, \chi)$ is the fundamental solution to the Laplace equation, $q^*(\xi, \chi)$ and $q(\xi)$ are the normal derivatives of $p^*(\xi, \chi)$ and $p(\xi)$, respectively. Here, p_c, is a constant value accounting for the no-flux condition of $\hat{p}$ across the fluid interface Γ, i.e.

$$\int_{\Gamma} \hat{q}(\chi) d\Gamma_{\chi} = 0 \tag{4.3.15}$$

By discretization of the surface boundary using standard boundary element approach, the above integral representation formula is converted in a linear matrix system of equation. In the discretization of the boundary Γ into N elements, the coordinates of each boundary point as well as the surface pressure and its normal derivative are described using B-splines functions. The local curvature at each point is evaluated using a fourth-order Lagrangian polynomial to minimize possible numerical oscillations. The unknown value of the interface pressure normal derivative, $\hat{q}$ is obtained after substituting the dynamic interface matching condition into the resulting matrix system. The value of $\hat{q}$ obtained is then substituted into the kinematic condition to find the interface displacement velocity for a given dissolution mass flux $\rho_g u_d$. In order to move the internal surface in time, a simple Euler approximation is used in integrating the surface normal displacement equation $\frac{ds}{dt} = V_n$, with V_n as the normal interface surface velocity.

The proposed B-spline BEM numerical scheme was verified by comparison its results with the evolution of the six tongues radial finger, without surface dissolution, studied experimentally by Paterson (1981), and numerically by Howison (1986) and Power (1994). The numerical results obtained for the fingering evolution, with the corresponding tip splitting, showed excellent agreement with previous numerical and experimental results, as well as analytical estimation of the finger's tip time evolution before the first splitting, showing asymptotical scale of $x \sim At^{0.6}$ (Almgren et al. 1993), for more details see Power et al. (2013).

The effect of dissolution is to erode the surface of the growing gas bubble. The effect is most pronounced in regions where the flow component normal to the bubble surface is small; most notably at the finger bases, where a stagnation point exists. Dissolution therefore works to thin the base of viscous fingers, eventually leading to their breaking at the base. These broken fingers move outwards due to convective forces in the surrounding fluid, and slowly normalise towards a circular shape due to the effect of surface tension, viscous sintering. With no further access to injected gas, the shed bubbles will eventually dissolve into the liquid. Power et al. (2013) reported a series of numerical examples showing the dissolution-driven breaking of viscous fingers.

We model the displacement of the brine of mobility $M = 5 \times 10^{-5}$ m^3 h/kg and density $p_l = 1.2 \times 10^3$ kg/m^3 by the CO_2 gas of lower mobility injected at a constant flux rate $Q = 0.5$ m^3/h. As previously reported by Kneafsey and Pruess (2009), in the case of CO_2-brine convectively enhances dissolution, a constant dissolution flux of the gas into the liquid is expected, here we used a constant rate $R = \rho_g u_d = 3.6 \times 10^{-3}$ kg/(m^2 h). Besides, according to Hele–Shaw–Chouke formulation, used in our simulations, an effective surface tension larger than the molecular surface tension needs to be considered in order to approximate the corresponding fingering evolution. The molecular surface tension of an open CO_2−brine interface varies due to temperature and pressure, but is of the order 0.02 to 0.07 kg m s^{-2}; see Bachu and Bennion (2009), here we used an effective surface tension $\gamma = 0.25$ kg m s^{-2}. Figure 4.10a shows the obtained fingers evolution for the above set of values corresponding to a CO_2-brine immiscible displacement when an initial irregular disturbance defined by $r = r_0 \cos((3/\sqrt{\pi})\theta^{3/2})$ is imposed where r is the radial distance from the origin.

As expected, a number of irregular fingering features are generated where it can be observed that the finger bases remain stationary, and fingers bifurcate when they grow to be sufficiently wide. Note that of the nine initial crests, only the fingers resulting three widest crests bifurcate immediately; the remaining fingers must grow and spread before the critical length scale is reached. Here the thinning of fingers due to the effect of dissolution is clearly visible at the bases, especially at the base of the higher-frequency disturbances.

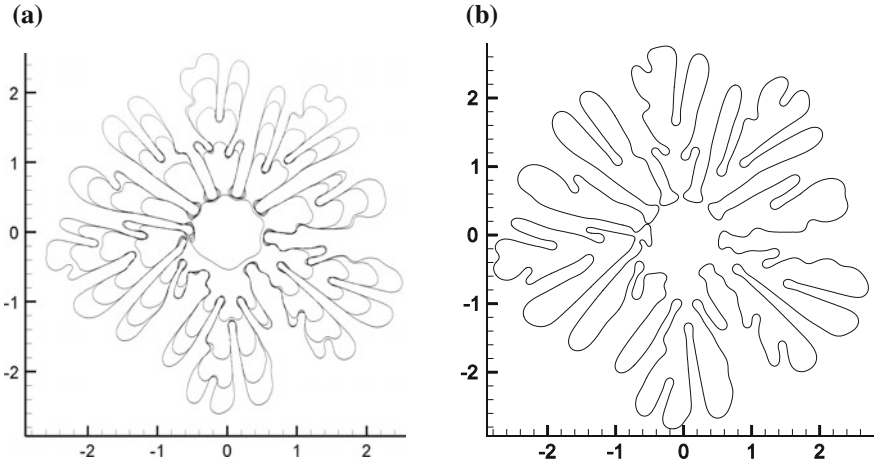

Fig. 4.10 **a** Fingering evolution before breaking, **b** fingering breaking (t = 22 h) by dissolution effect

The thinning of fingers at the base leads to breaking of the first finger at t = 22.0 h. These broken fingers rapidly re-grow towards the shed bubbles which will be split by the growing finger, further increasing the long-term rate of dissolution.

4.4 Example Case Studies

Auli Niemi, Zhibing Yang, Dorothee Rebscher, Bruno Figueiredo, Victor Vilarrasa, Jan Lennard Wolf and Franz May

In this chapter short example case studies are presented concerning modeling of real or proposed CO_2 injection sites. We start by exemplifying modeling of large scale storage sites by various methods and then proceed to examples addressing modeling of coupled hydro-chemical and hydro-mechanical processes.

4.4.1 Modeling of Large Scale Systems

Auli Niemi and Zhibing Yang

Predictions concerning the performance of large scale CO_2 storage systems involve, among other things, (1) estimating the induced pressure increase from the injection, to assure that it does not exceed the maximum allowed pressure tolerated by the formation and (2) estimating the CO_2 migration, to assure that the injected CO_2 does not get transported beyond allowable limits. When making such predictions, a number of uncertainties exist, ranging from uncertainties from data availability to the uncertainties arising from the use of different models and their underlying assumptions. To avoid errors arising from the use of specific models, Yang et al. (2015) and Tian et al. (2016) developed an approach to use a set of models of increasing complexity for modeling large scale sites and their performance in the long term. Yang et al. (2015) addressed the Dalders Monocline formation in the Baltic Sea, which site under the assumptions and injection scenarios tested showed to be pressure limited. Tian et al. (2016) in turn modeled the South Scania, Sweden, site, which under the investigated conditions and injection configurations was found to be migration limited.

The benefit of using models of increased complexity and accuracy is twofold. First, the use of several models obviously increases the level of confidence to model predictions, if several models with different simplifications and assumptions give similar results. Second, the use of models of increasing complexity can be useful

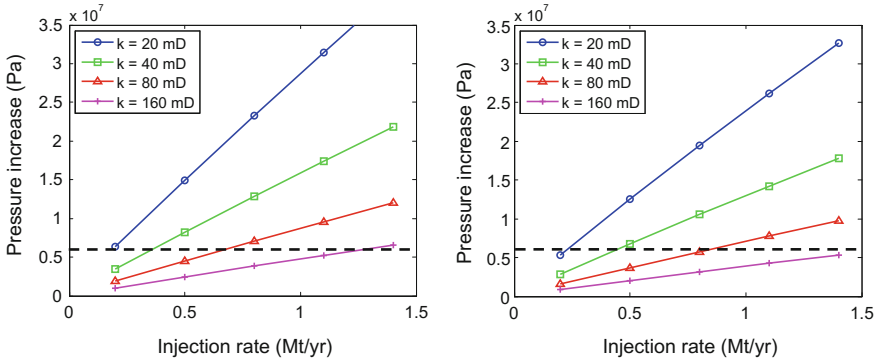

Fig. 4.11 Sensitivity of pressure increase to the permeability of the formation based on the preliminary simulations with a semi-analytical model. The distance from the injection well to the boundary is 5 km (*left panel*) and 25 m (*right panel*). The *dashed line* indicates the maximum allowed pressure increase (Yang et al. 2015)

when the simpler models are used to obtain first order-of-magnitude estimates and their results then used to guide the model scenarios for the more complex and computationally demanding models.

To exemplify, Yang et al. (2015) used the semi-analytical approach by Mathias et al. (2011) (see Sect. 4.1.3) to get the first estimates of the maximum allowed injection rate not to exceed the maximum allowed pressure and to carry out parameter sensitivity studies concerning the impact of variations in layer thickness, permeability, boundary conditions, etc. An example of the effect of permeability and distance to no-flow boundary (representing an impermeable fault) on pressure increase induced by a given injection rate is shown in Fig. 4.11. The next step was to use a more complicated but still somewhat simplified numerical model based on the vertical equilibrium assumption (e.g. Gasda et al. 2009, see also Sect. 4.1.2). This model, while still having simplifications in comparison to a 'full physics' high-fidelity model (Sect. 4.1.1), can give estimates of plume spreading, along with the information on pressure increase. The results from this model were then used to guide selecting the most detailed scenarios for the high-fidelity 'full-physics' modeling, carried out with the massively parallel TOUGH-MP simulator. Figure 4.12 shows example results of pressure plume evolution and spreading of the plume as simulated with the two models. Firstly, it can be seen that similar trends are observed in the results from the two models, regardless of the differences in their underlying assumptions. Secondly, it can be seen that the extent of the domain of the increased pressure is far more extensive than that of the CO_2 plume. For more discussions concerning the case study, the reader is referred to Yang et al. (2015) and for another example for a fundamentally different system to Tian et al. (2016).

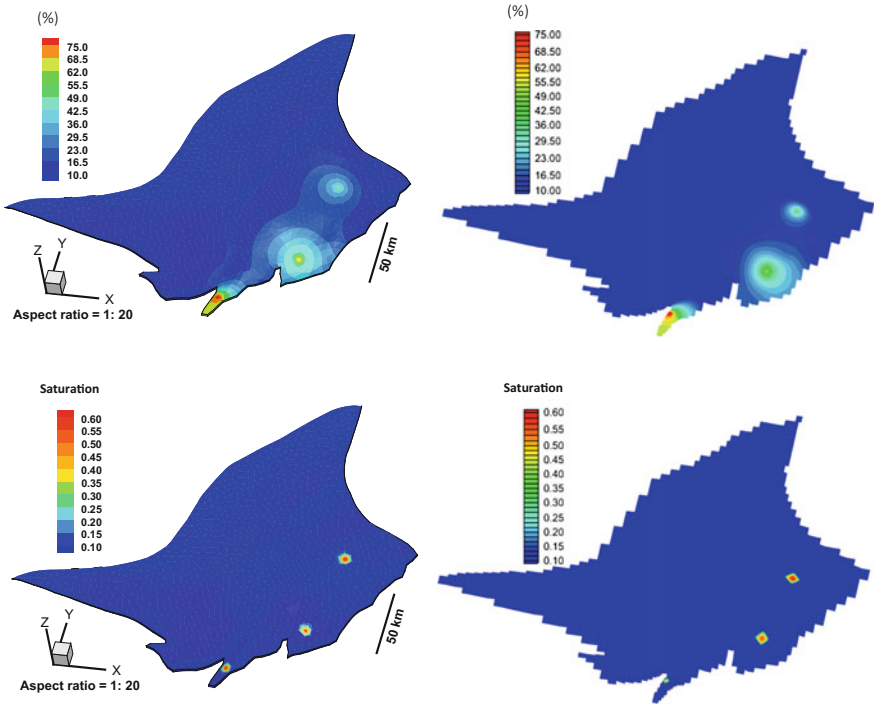

Fig. 4.12 Simulated overpressure distribution in percentage of the initial pressure (*upper panels*) as calculated with the VE model (*left*) and 3D TOUGH/MP (*right*) along with the simulated plume extent as expressed as depth averaged saturation distribution at 50 years after the start of injection (*lower panels*) with VE model (*left*) and TOUGH/MP (*right*). The injection rate is 0.5, 0.5 and 0.2 Mt/year from the three wells (Yang et al. 2015)

4.4.2 Modeling of Coupled Hydro-Geochemical Processes

Dorothee Rebscher, Jan Lennard Wolf and Franz May

Prominent computational tools for geochemical reaction modeling include CrunchFlow (Steefel 2009), Geochemist's Workbench (Bethke and Yeakel 2014), HST3D (Kipp 1997), together with PHREEQC forming PHAST (Parkhurst et al. 2010), HYTEC (van der Lee et al. 2003), HYDROGEOCHEM (Yeh and Tsai 2013), ORCHESTRA (Meeussen 2003), OpenGeoSys (Kolditz et al. 2012a) together with external geochemical solvers like IPHREEQC, open-source PFLOTRAN (Hammond et al. 2007; Lichtner et al. 2015), STOMP (White et al. 2012) with the reactive transport package ECKEChem (White and McGrail 2005), TOUGHREACT (Xu et al. 2014; Wei et al. 2015), and their derivatives or enhanced versions. Overviews of the capabilities of reactive transport codes in the subsurface are provided e.g. by Steefel et al. (2015), Zhang et al. (2012). Over the

years, numerous program testing, benchmark tests, as well as case studies have been performed for a wide range of coupled THMC processes (MacQuarrie and Mayer 2005; Kolditz et al. 2012b, 2015). In recent years, increased attention has been paid to the subject of CO_2 storage in deep saline sandstone reservoirs and the associated geochemical reactions (e.g. Balashov et al. 2013).

In the following, we will present an example of coupled hydro-geochemical modeling to investigate the geochemical effects in a proposed small scale CO_2 injection experiment at the pilot injection site Heletz, Israel (Niemi et al. 2016), where an impurity gas (in this case SO_2) is included in the injected gas stream. In the case of impurity gases, the geochemical effects are of particular interest.

In general, the scope of such simulations is to enhance the understanding of flow and transport of impure CO_2 and brine, and to investigate the induced chemical reactions and associated changes in the reservoir, such as porosity, permeability, pH value, and mineral composition. Coupling of transport and chemistry provides insights into their interdependency and helps to test the design, including inhibiting the release of noxious H_2S to the surface, which may be caused by SO_2 disproportionation reactions in a CO_2–SO_2–H_2O mixture. Special attention should be given to potential impacts on groundwater. Decrease in pH values due to the entry of CO_2 and/or SO_2 into an aquatic solution and resulting changes of geochemical equilibriums can be expected, e.g. added stress on the environment caused by this acidification. Some geochemical conversions are certainly expected, for instance the formation of solid carbonate ensuring mineral trapping of CO_2, as a result of CO_2 dissolved in water reacting with the reservoir rock. Other implications caused by chemical reactions are also of concern, like the release of contaminants, mainly metals, during chemical reactions. These effects have to be considered site-specifically in risk assessments, preventive actions, and remediation plans.

TOUGHREACT (Xu et al. 2006) code and its parallel version V3.0-OMP is used for the modeling of the example case study. The multi-component, multiphase flow in the porous media is first calculated by the general-purpose numerical simulation program TOUGH2. This code simulates fluid flow in liquid and gaseous phases, and the transitions between the phases, occurring under pressure, viscous, and gravity forces according to Darcy's law (Pruess et al. 1999). As an equation of state module, the fluid property model ECO_2N is used, which was especially developed for geological sequestration of CO_2 in saline aquifers, handling both aqueous and CO_2-rich phases (Pruess 2005). Thermodynamic and thermo-physical properties of H_2O–NaCl–CO_2 mixtures are given for appropriate temperature, pressure, and salinity ranges, i.e. $10\ °C \leq T \leq 110\ °C$, $P \leq 60$ MPa, and salinity up to full halite saturation, thus covering the conditions of the storage reservoir at Heletz with a temperature of 66 °C, a pressure of 14.7 MPa, and a salinity of 0.055 (Niemi et al. 2016). Part of the TOUGH suite of codes is the TOUGHREACT code, a reactive fluid flow and geochemical transport simulator for investigating reactive chemistry in both aqueous and gaseous phases (Xu et al. 2006). The code is well established, successfully applied in numerous case studies and various code comparison studies, e.g. Steefel et al. (2015). The parallel version TOUGHREACT V3.0-OMP provides the option of including SO_2 as a trace gas,

where SO_2 does not have to be injected as SO_2 dissolved in an additional saline fluid phase with the composition of the native brine. The latter more auxiliary method is often applied while using geochemical transport models, including the previous versions of TOUGHREACT.

At the Heletz pilot site (Niemi et al. 2016) a push-pull experiment with impurity gases is planned to be carried out. This is a typical example where complex coupled hydro-geochemical effects can be expected. The site geology, presented in detail in (Niemi et al. 2016), consists of sandstone reservoir layers with a cumulative thickness of approximately 20 m, located at depths of about 1650 m. Details of the modeling are explained in (Rebscher et al. 2015, 2014; Wolf et al., in press) and only some example results are presented here.

A basic 2D radial symmetric model on a field scale was constructed with a total of 3700 cells, representing three sandstone layers, adjacent by two shale layers. In the vertical, each of these five layers is portrayed by 3, 3, 9, 8, and 20 cells, respectively, their heights ranging layer dependent from about 0.36–1.4 m, with a cumulative height of 18 m. An incremental value of 1.06 for the horizontal grid sizes gives a higher discretization close to the injection well to obtain improved accuracy, resulting in horizontal cell sizes from 0.18 to 57 m with increasing distance to the well, covering 4000 m in total. Material parameters are based on Niemi et al. (2016) with permeabilities of about 10^{-13} and 10^{-15} m^2 for the sandstone and shale layers, respectively. Porosities vary from 10 to 20 %. The initial mineral composition of the sandstone is taken as follows: quartz is the prominent primary mineral with a volume fraction of almost 70 %. The primary carbonate of interest is calcite $CaCO_3$ with 3.7 %, secondary carbonates are ankerite, e.g. $CaFe(CO_3)_2$, dolomite $CaMg(CO_3)_2$, and siderite $FeCO_3$. Further primary minerals are orthoclase $KAlSi_3O_8$ and albite $NaAlSi_3O_8$ with 12 and 2.5 % and the clay minerals illite, e.g. $K_{0.85}Al_{2.85}Si_{3.15}O_{10}(OH)_2$, kaolinite $Al_2Si_2O_5(OH)_4$, and chlorite $(Mg, Fe)_3(Si, Al)_4O_{10}$, with 38.8, 32, and 14 % respectively. A secondary feldspar is anorthite $Ca(Al_2Si_2)O_8$.

The simulated injection scenario represents a potential schedule for injecting the binary mixture CO_2 to SO_2 in relation of 97 % to 3 %. The injection phase with a rate of approximately 0.28 kg/s for the first 100 h is followed by a relaxation phase of 144 h. During a shorter second injection phase, CO_2 saturated water is injected at a rate of 1 kg/s. All three phases together last 330 h, i.e. about 2 weeks. In the model, the injection occurs within the bottom cell of the sandstone layer A, located in the lower left corner of Fig. 4.13.

Both plots in this figure illustrate the situation after the recovery phase, i.e. after 244 h. It is evident that the area affected by the push–pull experiment is restricted to the vicinity of the injection point. As expected, the injection of the CO_2 to SO_2 mixture affects a strong decrease in pH value. Dissolving all the carbonate results with these initial mineral conditions in a slight decrease of porosity within a spatial range of about 3 m, because the precipitation of anhydrite features a higher molar volume compared to the one of dissolving calcite. Here, the impurity SO_2

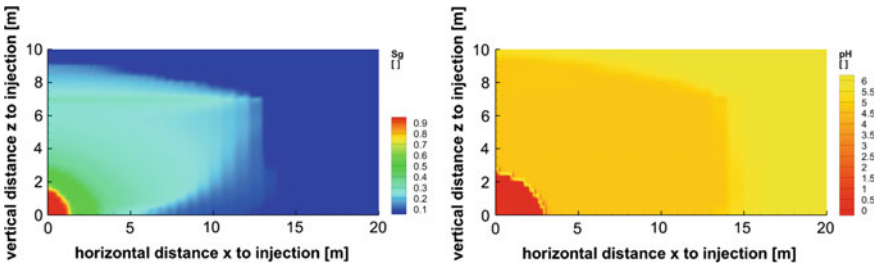

Fig. 4.13 Spatial distribution of CO_2 gas saturation (*left*) and Ph value (*right*) after the injection of 105 kg CO_2 to SO_2 in relation of 97 % to 3 % within 100 h, followed by a relaxation phase of 144 h; the diagrams show the whole vertical extent of 18 m of the five layer model, but only 20 m around the injection site in the horizontal direction (Rebscher et al. 2014)

preferentially dissolves into the aqueous phase due the higher solubility compared to CO_2. The higher aqueous SO_2 concentration and subsequently the higher reactivity zone is therefore constrained within the lower sandstone layer A, i.e. the lowest 7 m in Fig. 4.13. The resulting depleted supercritical CO_2 phase on the other hand reaches horizontal distances of about 15 and 10 m in the vertical, as can be seen in the spatial distributions of gas saturation S_g and pH value in Fig. 4.13. The carbonate dissolution induced by the decrease in pH value changes the porosity. Depending on the initial mineral composition of the rock, especially on the initial content of calcium in the minerals calcite ($CaCO_3$) and ankerite ($CaFe(CO_3)_2$), either a net increase or a net decrease in porosity, and hence in permeability, occurs (Wolf et al. in press).

4.4.3 Modeling of Coupled Hydro-Mechanical Systems

Bruno Figueiredo, Victor Vilarrasa and Auli Niemi

Pioneering work on modeling **coupled hydro-mechanical (HM)** processes has been carried out by e.g. Rutqvist and co-workers, including development of the TOUGH-FLAC code (Rutqvist 2011) that can handle such coupling. Examples of coupled hydro-mechanical modeling in CO_2 injection related applications include Rutqvist and Tsang (2002), Cappa and Rutqvist (2011, 2012), Castelletto et al. (2013), Goodarzi et al. (2015), Streit and Hillis (2004), Verdon et al. (2011), Vidal-Gilbert et al. (2010) and Vilarrasa et al. (2010b). As described in detail in Rutqvist (2011) in TOUGH-FLAC two established codes, namely TOUGH2 (Pruess et al. 1999) and FLAC 3D (Itasca 2012) that are linked to address the coupled hydro-mechanical processes for multiphase flow systems. TOUGH2 is used for solving multiphase flow and heat transport equations, and FLAC3D is used for solving geo-mechanical stress–strain equations. There are several other codes

that can address the coupled hydro-mechanical problem as well, including some tailored towards two-phase/multiphase flow problems. A comprehensive recent overview is also given in Rutqvist (2011, 2012) and will not be repeated here.

In terms of geological storage of CO_2, the major hydro-mechanical (HM) concerns calling for coupled HM modeling are maintaining caprock integrity to avoid CO_2 leakage (Vilarrasa et al. 2010b; Rutqvist et al. 2007), fault reactivation due to shear failure (Cappa and Rutqvist 2011; Rinaldi et al. 2015), and potential induced seismicity and fluid leakage (Vilarrasa and Carrera 2015a, b; Zoback and Gorelick 2012, 2015; Juanes et al. 2012; Rutqvist et al. 2007; Rutqvist and Tsang 2005; Hawkes et al. 2004).

In the following we will exemplify, following Figueiredo et al. (2015), the coupled HM modeling through a case study for potential fault reactivation due to CO_2 injection. The study site is Heletz site in Israel (Niemi et al. 2016), which is a test site for scientific CO_2 injection field experiments. The potential reservoir for CO_2 injection consists of three high-permeability sandstone layers, named K, W and A, separated by impermeable shale layers and overlain by a thick caprock. The confinement formations, located above the caprock and below the dolomite layer, are constituted essentially by limestone. The storage formation is intersected by two pre-existing sub-vertical normal faults (F1 and F2) on two opposite sides of the injection point.

A 5 km $\times$ 2.5 km vertical cross section with 1 m thickness was developed within the framework of TOUGH-FLAC code (Fig. 4.14). The mesh constitutes of 15,000 elements with refined elements close to the faults and storage formations. An injection rate for storage of 10 kg/s—which is more than ten times the injection rate used in the field experiments, to exaggerate the effect—was used in the simulations.

The difference in the results obtained by considering the actual three-layer storage formation in comparison to an equivalent single-layer formation is analyzed. No fault reactivation was observed in either case. It was also found that for the two cases the pore pressure evolution is similar, but the differences in the evolution of CO_2 saturation are significant, the latter being attributed to the differences in CO_2 spreading in a single versus three-layer storage layers. Fault slip displacement and changes in permeability were found not to be significant as the plastic shear strains mainly occur in a fault section that is only about 10 m in length, corresponding to the thickness of the storage formation.

Three key parameters were identified as important for the fault zone hydromechanics in association with CO_2 injection and storage: the offset of the storage layers across faults, the permeability of the confining formations and the thickness of the storage formation. The first key parameter was found to lead to an increase in CO_2 leakage through the caprock (Fig. 4.15). The second and third key parameters were found to have a direct relation with the length of the fault section reactivated by shear failure.

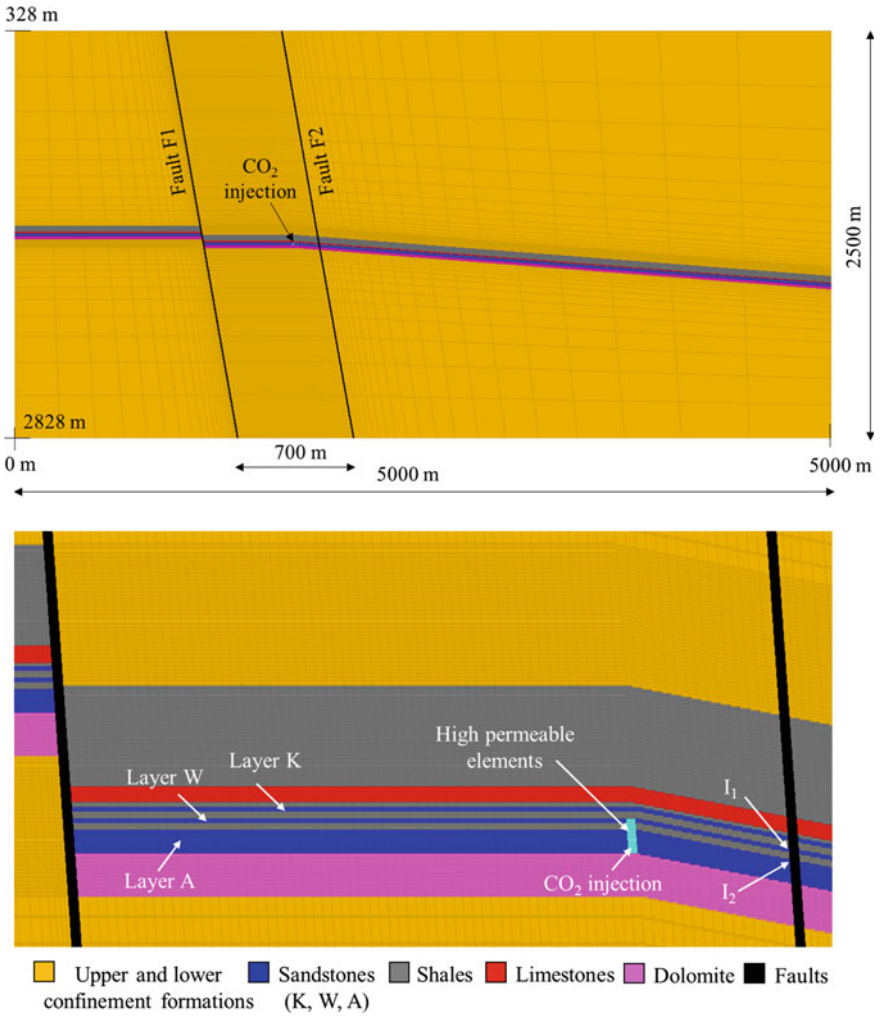

Fig. 4.14 Model mesh for the coupled simulations of CO_2 injection and faults slip (*above*) and a detail of the three-layer storage formation (the vertical scale has been expanded to display the storage details) (*below*) (Figueiredo et al. 2015)

Another example is the coupled **thermo-hydro-mechanical (THM) modeling** concerning liquid CO_2 injection presented in details in (Vilarrasa et al. 2013b, 2014). Most studies consider isothermal conditions. However, in general, CO_2 will reach the storage formation at a lower temperature than that corresponding to the geothermal gradient, especially at high flow rates (Paterson et al. 2008). A clear example of this can be found at e.g. In Salah, Algeria, where, even though CO_2 is injected at 35 °C at the surface, it reaches the storage formation at 50 °C (45 °C colder than the reservoir) (Bissell et al. 2011). Vilarrasa et al. (2013b) used

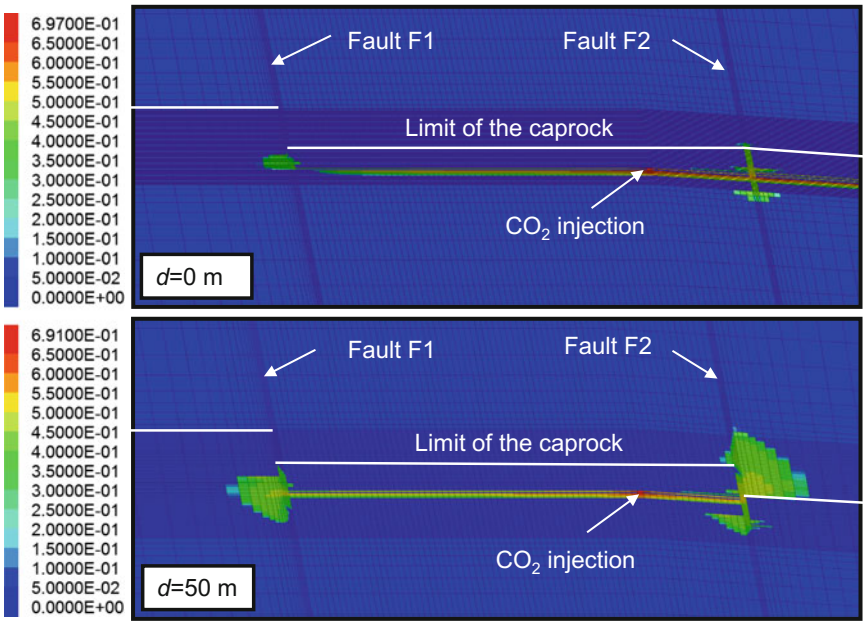

Fig. 4.15 CO_2 saturation (in %) obtained after 5 years of CO_2 injection with consideration of an offset d = 0 m (*above*) and 50 m (*below*) of the layers across the fault F2 (Figueiredo et al. 2015)

CODE_BRIGHT code for modeling the non-isothermal injection of 1 Mt/year of CO_2 at 20 °C in a reservoir with a mean temperature of 56 °C, to simulate liquid (cold and dense) CO_2 injection. Their simulation was coupled to mechanical deformation to address thermal stresses induced by the cold injection. Once liquid CO_2 enters into the reservoir, it heats up until thermal equilibrium with the geothermal gradient is reached, so that CO_2 evolves to supercritical conditions as it flows away from the well. As a result, the cold CO_2 region advances much behind the CO_2 plume interface. CO_2 remains in liquid conditions within the cold region, leading to a significantly higher density (around 900 kg/m^3) compared with the rest of the CO_2 plume (around 650 kg/m^3), where CO_2 stays in a supercritical state. This density difference affects overpressure as the denser fluid displaces a smaller amount of brine, thus inducing a slightly lower overpressure.

This lower overpressure is beneficial to maintain the geomechanical stability of the caprock and faults. However, cooling induces a thermal stress reduction that may lead to failure conditions (Gor et al. 2013). This thermal stress reduction is likely to induce shear failure conditions in the reservoir, which could explain part of the microseismic events detected at In Salah (Vilarrasa et al. 2015), or even the formation of hydraulic fractures in stiff reservoirs (Goodarzi et al. 2012). Nevertheless, the thermal stress reduction causes a stress redistribution around the cooled region leading to an increase of the horizontal stresses in the lower part of the caprock (Vilarrasa et al. 2013b). This stress redistribution tightens the caprock,

reducing the risk of CO_2 leakage across it. Thus, the thermal stress reduction induced by cooling should not be feared, but care should be taken to avoid inducing excessive microseismicity.

References

Almgren R, Dai WS, Hakim V (1993) Scaling behavior in anisotropic Hele–Shaw flow. Phys Rev Lett 71:3461–3464

Andersen O, Gasda SE, Nilsen HM (2015) Vertically averaged equations with variable density for CO_2. Transp Porous Media 107:95–127

Bachu S, Bennion DB (2009) Interfacial tension between CO_2, freshwater, and brine in the range of pressure from (2 to 27) MPa, temperature from (20 to 125) °C, and water salinity from (0 to 334,000) mg L^{-1}. J Chem Eng Data 54:765–775

Balashov VN, Guthrie GD, Hakala JA, Lopano CL, Rimstidt JD, Brantley SL (2013) Predictive modeling of CO_2 sequestration in deep saline sandstone reservoirs: impacts of geochemical kinetics. Appl Geochem 30:41–56

Bethke C, Yeakel S (2014) Geochemist's workbench: release 10.0 reaction modeling guide. Aqueous Solutions LLC, Champaign

Bissell RC, Vasco DW, Atbi M, Hamdani M, Okwelegbe M, Goldwater MH (2011) A full field simulation of the in Salah gas production and CO_2 storage project using a coupled geo-mechanical and thermal fluid flow simulator. In: Energy procedia, 10th international conference on greenhouse gas control technologies, vol 4, pp 3290–3297

Bronstein IN, Semedjajew KA (1977) Taschenbuch der Mathematik (Handbook of mathematics). Harri Deutsch, Frankfurt

Buckley SE, Leverett MC (1941) Mechanism of fluid displacement in sands. Trans AIME 146:107–116

Cabral JJSP, Wrobel LC, Brebbia CA (1990) A BEM formulation using B-splines: I—uniform blending functions. Eng Anal Bound Elem 7:136–144

Cao H (2002) Development of techniques for general purpose simulators. Stanford University

Cappa F, Rutqvist J (2011) Impact of CO_2 geological sequestration on the nucleation of earthquakes. Geophys Res Lett 38:L17313

Cappa F, Rutqvist J (2012) Seismic rupture and ground accelerations induced by CO_2 injection in the shallow crust. Geophys J Int 190:1784–1789

Castelletto N, Gambolati G, Teatini P (2013) Geological CO_2 sequestration in multi-compartment reservoirs: geomechanical challenges. J Geophys Res Solid Earth 118:2417–2428

Cavanagh AJ, Haszeldine RS, Nazarian B (2015) The Sleipner CO_2 storage site: using a basin model to understand reservoir simulations of plume dynamics. First Break 33:61–68

Celia MA, Nordbotten JM (2009) Practical modeling approaches for geological storage of carbon dioxide. Ground Water 47:627–638

Chang KW, Hesse MA, Nicot J-P (2013) Reduction of lateral pressure propagation due to dissipation into ambient mudrocks during geological carbon dioxide storage. Water Resour Res 49:2573–2588

Chen Y, Durlofsky LJ, Gerritsen M, Wen XH (2003) A coupled local–global upscaling approach for simulating flow in highly heterogeneous formations. Adv Water Resour 26:1041–1060

Chuoke RL, van Meurs P, van der Poel C (1959) The instability of slow, immiscible, viscous liquid–liquid displacements in permeable media. Trans. AIME 216, pp 188–194

Cihan A, Zhou Q, Birkholzer JT (2011) Analytical solutions for pressure perturbation and fluid leakage through aquitards and wells in multilayered-aquifer systems. Water Resour Res 47: W10504

Class H, Ebigbo A, Helmig R, Dahle HK, Nordbotten JM, Celia MA, Audigane P, Darcis M, Ennis-King J, Fan Y, Flemisch B, Gasda SE, Jin M, Krug S, Labregere D, Beni AN, Pawar RJ, Sbai A, Thomas SG, Trenty L, Wei L (2009) A benchmark study on problems related to CO_2 storage in geologic formations. Comput Geosci 13:409–434

Daripa P, Pasa G (2008) Hydrodynamic stability of multi-layer Hele–Shaw flows. J Stat Mech Theory Exp 2008:P12005

de Marsily G (1986) Quantitative hydrogeology: groundwater hydrology for engineers. Academic Press, London

Degregoria AJ, Schwartz LW (1986) A boundary-integral method for two-phase displacement in Hele–Shaw cells. J Fluid Mech 164:383

Dentz M, Carrera J (2003) Effective dispersion in temporally fluctuating flow through a heterogeneous medium. Phys Rev E 68:36310

Dentz M, Tartakovsky DM (2008) Abrupt-interface solution for carbon dioxide injection into porous media. Transp Porous Media 79:15–27

Durlofsky LJ, Efendiev Y, Ginting V (2007) An adaptive local–global multiscale finite volume element method for two-phase flow simulations. Adv Water Resour 30:576–588

Edwards D, Brenner H, Wasan D (1991) Interfacial transport processes and rheology. Butterworth-Heinemann, Boston

Elenius MT, Nordbotten JM, Kalisch H (2014) Convective mixing influenced by the capillary transition zone. Comput Geosci 18:417–431

Emami-Meybodi H, Hassanzadeh H (2015) Two-phase convective mixing under a buoyant plume of CO_2 in deep saline aquifers. Adv Water Resour 76:55–71

Ferguson G, Woodbury AD (2005) Thermal sustainability of groundwater-source cooling in Winnipeg, Manitoba. Can Geotech J 42:1290–1301

Figueiredo B, Tsang C-F, Rutqvist J, Bensabat J, Niemi A (2015) Coupled hydro-mechanical processes and fault reactivation induced by CO_2 Injection in a three-layer storage formation. Int J Greenhouse Gas Control 39:432–448

Freifeld B, Zakim S, Pan L, Cutright B, Sheu M, Doughty C, Held T (2013) Geothermal energy production coupled with CCS: a field demonstration at the SECARB Cranfield Site, Cranfield, Mississippi, USA. Energy Procedia 37:6595–6603

Fu X, Cueto-Felgueroso L, Bolster D, Juanes R (2015) Rock dissolution patterns and geochemical shutdown of—brine–carbonate reactions during convective mixing in porous media. J Fluid Mech 764:296–315

Garcia JE, Pruess K (2003) Flow instabilities during injection of into saline aquifers. In: Presented at the TOUGH symposium, Berkeley, CA, USA

Gasda SE, Nordbotten JM, Celia MA (2009) Vertical equilibrium with sub-scale analytical methods for geological CO_2 sequestration. Comput Geosci 13:469–481

Gasda SE, Nordbotten JM, Celia MA (2011) Vertically averaged approaches for CO_2 migration with solubility trapping. Water Resour Res 47:W05528

Gasda SE, Nordbotten JM, Celia MA (2012) Application of simplified models to CO_2 migration and immobilization in large-scale geological systems. Int J Greenhouse Gas Control 9:72–84

Ghesmat K, Hassanzadeh H, Abedi J (2011) The impact of geochemistry on convective mixing in a gravitationally unstable diffusive boundary layer in porous media: CO_2 storage in saline aquifers. J Fluid Mech 673:480–512

Glimm J, Grove JW, Li X, Zhao N (1999) In: Chen G-Q, DiBenedetto E (eds) Simple front tracking, vol 238. Am. Math. Soc, Providence, pp 133–149

Goodarzi S, Settari A, Keith D (2012) Geomechanical modeling for CO_2 storage in Nisku aquifer in Wabamun Lake area in Canada. Int J Greenhouse Gas Control 10:113–122

Goodarzi S, Settari A, Zoback MD, Keith DW (2015) Optimization of a CO_2 storage project based on thermal, geomechanical and induced fracturing effects. J Pet Sci Eng 134:49–59

Gor GY, Elliot TR, Prévost JH (2013) Effects of thermal stresses on caprock integrity during CO_2 storage. Int J Greenhouse Gas Control 12:300–309

Gorell S, Homsy G (1983) A theory of the optimal policy of oil recovery by secondary displacement processes. SIAM J Appl Math 43:79–98

Häfner F, Sames D, Voigt H.-D (1992) Wärme- und Stofftransport. Springer-Lehrbuch, Berlin
Hammond G, Lichtner P, Lu C (2007) Subsurface multiphase flow and multicomponent reactive transport modeling using high-performance computing. J Phys Conf Ser 78:12025
Hassanzadeh H, Pooladi-Darvish M, Elsharkawy AM, Keith DW, Leonenko Y (2008) Predicting PVT data for CO_2–brine mixtures for black-oil simulation of CO_2 geological storage. Int J Greenhouse Gas Control 2:65–77
Hawkes CD, McLellan PJ, Zimmer U, Bachu S (2004) Geomechanical factors affecting geological storage of CO_2 in depleted oil and gas reservoirs: risks and mechanisms. In: Proceedings of gulf rocks 2004, presented at the sixth North America rock mechanics symposium (NARMS): rock mechanics across borders and disciplines, Houston, TX, USS
Helmig R (1997) Multiphase flow and transport processes in the subsurface: a contribution to the modeling of hydrosystems. Springer, Berlin, p 367
Hesse MA, Orr FM, Tchelepi HA (2008) Gravity currents with residual trapping. J Fluid Mech 611:35–60
Hickernell JF, Yortsos YC (1986) Linear stability of miscible displacement processes in porous media in the absence of dispersion. Stud Appl Math 74:93–115
Hidalgo JJ, Carrera J (2009) Effect of dispersion on the onset of convection during CO_2 sequestration. J Fluid Mech 640:441
Hidalgo JJ, Carrera J, Dentz M (2009a) Steady state heat transport in 3D heterogeneous porous media. Adv Water Resour 32:1206–1212
Hidalgo JJ, Carrera J, Medina A (2009b) Role of salt sources in density-dependent flow. Water Resour Res 45:W05503
Hidalgo, JJ, Dentz M, Cabeza Y, Carrera J (2015) Dissolution patterns and mixing dynamics in unstable reactive flow. Geophys Res Lett 42:6357–6364
Hidalgo JJ, Slooten LJ, Medina A, Carrera J (2005) A Newton–Raphson based code for seawater intrusion modelling and parameter estimation. In: Araguas L, Custodio E, Manzano M (eds) Groundwater and saline intrusion: selected papers from the 18th salt water in-trusion meeting, 18th SWIM, Cartagena, 2004. IGME, pp 111–120
Homsy GM (1987) Viscous fingering in porous media. Annu Rev Fluid Mech 19:271–311
Houseworth JE (2012) Matched boundary extrapolation solutions for CO_2 well-injection into a saline aquifer. Transp Porous Media 91:813–831
Howison SD (1986) Fingering in Hele–Shaw cells. J Fluid Mech 167:439–453
Huang AB, Chikhliwala ED, Yortsos YC (1984) Linear stability analysis of immiscible displacement including continuously changing mobility and capillary effects: part II—general basic flow profiles. SPE 13163, Society of Petroleum Engineers, Dallas, Tex
Huang H, Meakin P (2008) Three-dimensional simulation of liquid drop dynamics within unsaturated vertical Hele–Shaw cells. Water Resour Res 44:10
Huang P-M, Wang M-K, Chiu C-Y (2005) Soil mineral–organic matter–microbe interactions: impacts on biogeochemical processes and biodiversity in soils. Pedobiologia 49:609–635
Huang X, Bandilla KW, Celia MA (2014) Basin-scale modeling of CO_2 storage using models of varying complexity. Int J Greenhouse Gas Control 20:73–86
IPCC (2005) IPCC special report on carbon dioxide capture and storage. In: Prepared by working group III of the intergovernmental panel on climate change. Cambridge University Press, Cambridge, New York
Itasca (2012) FLAC3D, fast lagrangian analysis of continua in 3 dimensions. Version 5.0. Minneapolis, Minnesota
Jackson SJ, Stevens D, Giddings D, Power H (2015a) Dynamic-wetting effects in finite-mobility-ratio Hele–Shaw flow. Phys Rev E 92:23021
Jackson SJ, Stevens D, Power H, Giddings D (2015b) A boundary element method for the solution of finite mobility ratio immiscible displacement in a Hele–Shaw cell. Int J Numer Methods Fluids 78:521–551
Jessen K, Kovscek AR, Orr FM Jr (2005) Increasing CO_2 storage in oil recovery. Energy Convers Manag 46:293–311

Juanes R, Hager BH, Herzog HJ (2012) No geologic evidence that seismicity causes fault leakage that would render large-scale carbon capture and storage unsuccessful. Proc Natl Acad Sci USA 109:E3623 (author reply E3624)

Juanes R, MacMinn CW, Szulczewski ML (2010) The footprint of the CO_2 plume during carbon dioxide storage in saline aquifers: storage efficiency for capillary trapping at the basin scale. Transp Porous Media 82:19–30

Juanes R, Spiteri EJ, Orr FM, Blunt MJ (2006) Impact of relative permeability hysteresis on geological CO_2 storage. Water Resour Res 42:W12418

Kipp KL (1997) Guide to the revised heat and solute transport simulator: HST3D—version 2 (No. Water-Resources Investigations Report 97-4157). U.S. Geological Survey, Denver

Knabner P, Frolkovic P (1996) Consistent velocity approximation for finite volume or element discretizations of density driven flow in porous media. In: Aldama AA, Aparicio J, Brebbia CA, Gray WG, Herrera I, Pinder G (eds) Computational methods in subsurface flow and transport problems, computational methods in water resources XI. Computational Mechanics, Southamptonm, pp 93–100. Southampton

Kneafsey TJ, Pruess K (2009) Laboratory flow experiments for visualizing carbon dioxide-induced, density-driven brine convection. Transp Porous Media 82:123–139

Kolditz O (2001) Non-linear flow in fractured rock. Int J Numer Methods Heat Fluid Flow 11:547–575

Kolditz O, Bauer S, Bilke L, Böttcher N, Delfs JO, Fischer T, Görke UJ, Kalbacher T, Kosakowski G, McDermott CI, Park CH, Radu F, Rink K, Shao H, Shao HB, Sun F, Sun YY, Singh AK, Taron J, Walther M, Wang W, Watanabe N, Wu Y, Xie M, Xu W, Zehner B (2012a) OpenGeoSys: an open-source initiative for numerical simulation of thermo-hydro-mechanical/chemical (THM/C) processes in porous media. Environ Earth Sci 67:589–599

Kolditz O, Görke U-J, Shao H, Wang W (eds) (2012b) Thermo-hydro-mechanical-chemical processes in porous media. Lecture notes in computational science and engineering. Springer, Berlin

Kolditz O, Shao H, Wang W, Bauer S (eds) (2015) Thermo-hydro-mechanical-chemical processes in fractured porous media: modelling and benchmarking closed-form solutions, terrestrial environmental sciences. Springer, Cham

Kueper BH, McWhorter DB (1992) The use of macroscopic percolation theory to construct large-scale capillary pressure curves. Water Resour Res 28:2425–2436

Lake LW (1989) Enhanced oil recovery. Prentice Hall, New Jersey

Landman AJ, Schotting RJ (2007) Heat and brine transport in porous media: the Oberbeck–Boussinesq approximation revisited. Transp Porous Media 70:355–373

Lenormand R, Touboul E, Zarcone C (1988) Numerical models and experiments on immiscible displacements in porous media. J Fluid Mech 189:165–187

Lichtner PC, Hammond GE, Lu C, Karra S, Bisht G, Andre B, Mills R, Kumar J (2015) PFLOTRAN user manual, a massively parallel reactive flow and transport, model for describing surface and subsurface processes. Technical Report No. LA-UR-15-20403, Los Alamos National Laboratory, Los Alamos, NM, p 195

Lu C, Lichtner PC (2007) High resolution numerical investigation on the effect of convective instability on long term CO_2 storage in saline aquifers. J Phys Conf Ser 78:12042

MacMinn CW, Juanes R (2009) Post-injection spreading and trapping of CO_2 in saline aquifers: impact of the plume shape at the end of injection. Comput Geosci 13:483–491

MacMinn CW, Szulczewski ML, Juanes R (2011) CO_2 migration in saline aquifers. Part 2. Capillary and solubility trapping. J Fluid Mech 688:321–351

MacQuarrie KTB, Mayer KU (2005) Reactive transport modeling in fractured rock: a state-of-the-science review. Earth Sci Rev 72:189–227

Mathias SA, Gluyas JG, Martínez González, de Miguel GJ, Hosseini SA (2011) Role of partial miscibility on pressure buildup due to constant rate injection of CO_2 into closed and open brine aquifers. Water Resour Res 47:W12525

Mathias SA, Gluyas JG, Martínez González, de Miguel GJ, Bryant SL, Wilson D (2013) On relative permeability data uncertainty and CO_2 injectivity estimation for brine aquifers. Int J Greenhouse Gas Control 12:200–212

McDermott CI, Bond AE, Wang W, Kolditz O (2011) Front tracking using a hybrid analytical finite element approach for two-phase flow applied to supercritical CO_2. Transp Porous Media 90:545–573

Meakin P, Tartakovsky AM (2009) Modeling and simulation of pore-scale multiphase fluid flow and reactive transport in fractured and porous media. Rev Geophys 47:RG3002

Meeussen JCL (2003) ORCHESTRA: an object-oriented framework for implementing chemical equilibrium models. Environ Sci Technol 37:1175–1182

Neufeld JA, Hesse MA, Riaz A, Hallworth MA, Tchelepi HA, Huppert HE (2010) Convective dissolution of carbon dioxide in saline aquifers. Geophys Res Lett 37:L22404

Nicot J-P (2008) Evaluation of large-scale CO_2 storage on fresh-water sections of aquifers: an example from the Texas Gulf Coast Basin. Int J Greenhouse Gas Control 2:582–593

Niemi A, Bensabat J, Shtivelman V, Edlmann K, Gouze P, Luquot L, Hingerl F, Benson SM, Pezard PA, Rasmusson K, Liang T, Fagerlund F, Gendler M, Goldberg I, Tatomir A, Lange T, Sauter M, Freifeld B (2016) Heletz experimental site overview, characterization and data analysis for CO_2 injection and geological storage. Int J Greenhouse Gas Control 48:3–23

Niessner J, Hassanizadeh SM (2008) A model for two-phase flow in porous media including fluid–fluid interfacial area. Water Resour Res 44:W08439

Nilsen HM, Lie KA, Andersen O (2016) Robust simulation of sharp-interface models for fast estimation of CO_2. Comput Geosci 20:93–113

Nordbotten JM, Celia MA (2006) Similarity solutions for fluid injection into confined aquifers. J Fluid Mech 561:307–327

Nordbotten JM, Celia MA, Bachu S (2005) Injection and storage of CO_2 in deep saline aquifers: analytical solution for CO_2 plume evolution during injection. Transp Porous Media 58:339–360

Nordbotten JM, Flemisch B, Gasda SE, Nilsen HM, Fan Y, Pickup GE, Wiese B, Celia MA, Dahle HK, Eigestad GT, Pruess K (2012) Uncertainties in practical simulation of CO_2 storage. Int J Greenhouse Gas Control 9:234–242

Nordbotten JM, Michael AC (2011) Geological storage of CO_2: modeling approaches for large-scale simulation. Wiley, New Jersey

Obi EOI, Blunt MJ (2006) Streamline-based simulation of carbon dioxide storage in a North Sea aquifer. Water Resour Res 42:W03414

Olivella S, Gens Solé A, Carrera Ramírez J, Pérez Alonso, de Agreda E (1996) Numerical formulation for a simulator (CODE_BRIGHT) for the coupled analysis of saline media. Eng Comput 13:87–112

Parkhurst DL, Kipp KL, Charlton SR (2010) PHAST version 2-A program for simulating groundwater flow, solute transport, and multicomponent geochemical reactions. U.S. Geological Survey Techniques and Methods, 6-A35 (2010). Denver, Colo, p 25

Paterson L (1981) Radial fingering in a Hele Shaw cell. J Fluid Mech 113:513

Paterson L, Lu M, Connell L, Ennis-King JP (2008) Numerical modeling of pressure and temperature profiles including phase transitions in carbon dioxide wells. In: Presented at the SPE annual technical conference and exhibition, 21–24 Sept, Society of Petroleum Engineers, Denver, CO, USA

Pau GSH, Bell JB, Pruess K, Almgren AS, Lijewski MJ, Zhang K (2010) High-resolution simulation and characterization of density-driven flow in CO_2 storage in saline aquifers. Adv Water Resour 33:443–455

Power H (1994) The evolution of radial fingers at the interface between two viscous liquids. Eng Anal Bound Elem 14:297–304

Power H, Stevens D, Cliffe KA, Golin A (2013) A boundary element study of the effect of surface dissolution on the evolution of immiscible viscous fingering within a Hele–Shaw cell. Eng Anal Bound Elem 37:1318–1330

Power H, Wrobel LC (1995) Boundary integral methods in fluid mechanics. Computational Mechanics Publications, Southampton and Boston

Pruess K (2011) ECO2M: a TOUGH2 fluid property module for mixtures of water, NaCl, and CO_2, including super- and sub-critical conditions, and phase change between liquid and gaseous CO_2 (No. LBNL-4590E). Lawrence Berkeley National Laboratory, Berkeley

Pruess K (2005) ECO2N: a TOUGH2 fluid property module for mixtures of water, NaCl, and CO_2 (No. LBNL-57952). Lawrence Berkeley National Laboratory, Berkeley

Pruess K, García J, Kovscek T, Oldenburg C, Rutqvist J, Steefel C, Xu T (2004) Code intercomparison builds confidence in numerical simulation models for geologic disposal of CO_2. In: Energy, 6th international conference on greenhouse gas control technologies, vol 29, pp 1431–1444

Pruess K, Oldenburg CM, Moridis GJ (1999) TOUGH2 user's guide version 2 (No. LBNL–43134, 751729). Berkeley National Laboratory, Berkeley

Rasmusson M, Fagerlund F, Tsang Y, Rasmusson K, Niemi A (2015) Prerequisites for density-driven instabilities and convective mixing under broad geological CO_2 storage conditions. Adv Water Resour 84:136–151

Rebscher D, Wolf JL, Bensabat J, Niemi A (2015) Numerical simulations of the chemical impact of impurities on geological CO_2 storage—comparison between TOUGHREACT V2.0 and TOUGHREACT V3.0-OMP. In: Paper proceedings LBNL-190559, presented at the TOUGH symposium 2015, Lawrence, Berkeley National Laboratory, CA, USA, pp 493–500

Rebscher D, Wolf JL, Jung B, Bensabat J, Segev R, Niemi AP (2014) Effects of impurities in CO_2 spreading model development for field experiments in the framework of the CO2QUEST project. In: AGU fall meeting, abstr. 21

Riaz A, Hesse M, Tchelepi HA, Orr FM (2006) Onset of convection in a gravitationally unstable diffusive boundary layer in porous media. J Fluid Mech 548:87–111

Rinaldi AP, Vilarrasa V, Rutqvist J, Cappa F (2015) Fault reactivation during CO_2 sequestration: effects of well orientation on seismicity and leakage. Greenh Gas Sci Technol 5:645–656

Rutqvist J (2011) Status of the TOUGH-FLAC simulator and recent applications related to coupled fluid flow and crustal deformations. Comput. Geosci 37:739–750 (Transport of Unsaturated Groundwater and Heat Symposium 2009, TOUGH Symposium)

Rutqvist J (2012) The geomechanics of CO_2 storage in deep sedimentary formations. Geotech Geol Eng 30:525–551

Rutqvist J, Birkholzer J, Cappa F, Tsang C-F (2007) Estimating maximum sustainable injection pressure during geological sequestration of CO_2 using coupled fluid flow and geomechanical fault-slip analysis. Energy Convers Manag 48:1798–1807

Rutqvist J, Birkholzer JT, Tsang C-F (2008) Coupled reservoir–geomechanical analysis of the potential for tensile and shear failure associated with CO_2 injection in multilayered reservoir–caprock systems. Int J Rock Mech Min Sci 45:132–143

Rutqvist J, Tsang C-F (2005) Coupled hydromechanical effects of CO_2 injection. In: Apps JA, Tsang CF (eds) Developments in water science, underground injection science and technology. Elsevier, Amsterdam, pp 649–679

Rutqvist J, Tsang C-F (2002) A study of caprock hydromechanical changes associated with CO_2-injection into a brine formation. Environ Geol 42:296–305

Saaltink MW, Ayora C, Carrera J (1998) A mathematical formulation for reactive transport that eliminates mineral concentrations. Water Resour Res 34:1649–1656

Saaltink MW, Carrera J, Olivella S (2004) Mass balance errors when solving the convective form of the transport equation in transient flow problems. Water Resour Res 40:W05107

Schlumberger (2012) ECLIPSE technical description. Schlumberger, Sugar Land

Shamshiri H, Jafarpour B (2012) Controlled CO_2 injection into heterogeneous geologic formations for improved solubility and residual trapping. Water Resour Res 48:W02530

Singh VP, Cavanagh A, Hansen H, Nazarian B, Iding M, Ringrose PS (2010) Reservoir modeling of CO_2 plume behavior calibrated against monitoring data from Sleipner, Norway. In: Presented at the SPE annual technical conference and exhibition, Society of Petroleum Engineers, Florence, Italy

Slattery JC (1999) Advanced transport phenomena. Cambridge University Press, New York
Steefel CI (2009) CrunchFlow, software for modeling multicomponent reactive flow and transport, user's manual. Berkeley, Calif
Steefel CI, Appelo CAJ, Arora B, Jacques D, Kalbacher T, Kolditz O, Lagneau V, Lichtner PC, Mayer KU, Meeussen JCL, Molins S, Moulton D, Shao H, Šimůnek J, Spycher N, Yabusaki SB, Yeh GT (2015) Reactive transport codes for subsurface environmental simulation. Comput. Geosci 19:445–478
Streit JE, Hillis RR (2004) Estimating fault stability and sustainable fluid pressures for underground storage of CO_2 in porous rock. In: Energy, 6th international conference on greenhouse gas control technologies, vol 29, pp 1445–1456
Szulczewski ML, Hesse MA, Juanes R (2013) Carbon dioxide dissolution in structural and stratigraphic traps. J Fluid Mech 736:287–315
Thorenz C, Kosakowski G, Kolditz O, Berkowitz B (2002) An experimental and numerical investigation of saltwater movement in coupled saturated—partially saturated systems. Water Resour Res 38:1–5
Tian L, Yang Z, Fagerlund F, Niemi A (2016) Effects of permeability heterogeneity on CO_2 injectivity and storage efficiency coefficient. Greenh Gas Sci Technol 6:112–124
Tosaka N, Sugino R (1994) Boundary element analysis of moving boundary in Laplacian growth. In: Computational modeling of free and moving boundary problems II. Computational Mechanics Publication, Southampton
Tsang C-F (1991) Coupled hydromechanical-thermochemical processes in rock fractures. Rev Geophys 29:537–551
Unverdi SO, Tryggvason G (1992) A front-tracking method for viscous, incompressible, multi-fluid flows. J Comput Phys 100:25–37
van der Lee J, De Windt L, Lagneau V, Goblet P (2003) Module-oriented modeling of reactive transport with HYTEC. Comput Geosci 29:265–275
Verdon JP, Kendall J-M, White DJ, Angus DA (2011) Linking microseismic event observations with geomechanical models to minimise the risks of storing CO_2 in geological formations. Earth Planet Sci Lett 305:143–152
Vidal-Gilbert S, Tenthorey E, Dewhurst D, Ennis-King J, Van Ruth P, Hillis R (2010) Geomechanical analysis of the Naylor Field, Otway Basin, Australia: implications for CO_2 injection and storage. Int J Greenhouse Gas Control 4:827–839
Vilarrasa V, Bolster D, Dentz M, Olivella S, Carrera J (2010a) Effects of CO_2 compressibility on CO_2 storage in deep saline aquifers. Transp Porous Media 85:619–639
Vilarrasa V, Bolster D, Olivella S, Carrera J (2010b) Coupled hydromechanical modeling of CO_2 sequestration in deep saline aquifers. Int J Greenhouse Gas Control 2009(4):910–919
Vilarrasa V, Carrera J (2015a) Geologic carbon storage is unlikely to trigger large earthquakes and reactivate faults through which CO_2 could leak. Proc Natl Acad Sci USA 112:5938–5943
Vilarrasa V, Carrera J (2015b) Reply to Zoback and Gorelick: geologic carbon storage remains a safe strategy to significantly reduce CO_2 emissions. Proc Natl Acad Sci USA 112:E4511
Vilarrasa V, Carrera J, Bolster D, Dentz M (2013a) Semianalytical solution for plume shape and pressure evolution during CO_2 injection in deep saline formations. Transp Porous Media 97:43–65
Vilarrasa V, Olivella S, Carrera J, Rutqvist J (2014) Long term impacts of cold CO_2 injection on the caprock integrity. Int J Greenhouse Gas Control 24:1–13
Vilarrasa V, Rutqvist J, Rinaldi AP (2015) Thermal and capillary effects on the caprock mechanical stability at In Salah, Algeria. Greenh Gas Sci Technol 5:449–461
Vilarrasa V, Silva O, Carrera J, Olivella S (2013b) Liquid CO_2 injection for geological storage in deep saline aquifers. Int J Greenhouse Gas Control 14:84–96
Ward TJ, Cliffe KA, Jensen OE, Power H (2014a) Dissolution-driven porous-medium convection in the presence of chemical reaction. J Fluid Mech 747:316–349
Ward TJ, Jensen OE, Power H, Riley DS (2014b) High-Rayleigh-number convection of a reactive solute in a porous medium. J Fluid Mech 760:95–126

Wei X, Li W, Tian H, Li H, Xu H, Xu T (2015) THC-MP: high performance numerical simulation of reactive transport and multiphase flow in porous media. Comput Geosci 80:26–37

Weitz DA, Stokes JP, Ball RC, Kushnick AP (1987) Dynamic capillary-pressure in porous-media —origin of the viscous-fingering length scale. Phys Rev Lett 59:2967–2970

White MD, Bacon DH, McGrail BP, Watson DJ, White, SK, Zhang ZF (2012) Stomp subsurface transport over multiple phases: STOMP-CO_2 and Stomp-CO_2e Guide: version 1.0 (No. PNNL-21268). Pacific Northwest National Laboratory (PNNL), Richland

White MD, McGrail BP (2005) STOMP subsurface transport over multiple phases version 1.0 addendum: ECKEChem equilibrium-conservation-kinetic equation chemistry and reactive transport. United States Department of Energy, Washington, DC

Wilkinson D, Willemsen JF (1983) Invasion percolation: a new form of percolation theory. J Phys Math Gen 16:3365–3376

Wolf JL, Niemi A, Bensabat J, Rebscher D (in press) Benefits and restrictions of 2D reactive transport simulations of CO_2 and SO_2 co-injection into a saline aquifer using TOUGHREACT V3.0-OMP. Int J Greenhouse Gas Control

Xiaoping T, Juemin P, Junkai C (1997) Three dimensional simulation of unstable immiscible displacement in the porous medium. Appl Math Mech 18:81–89

Xu T, Sonnenthal E, Spycher N, Pruess K (2006) TOUGHREACT—a simulation program for non-isothermal multiphase reactive geochemical transport in variably saturated geologic media: applications to geothermal injectivity and CO_2 geological sequestration. Comput Geosci 32:145–165

Xu T, Sonnenthal E, Spycher N, Zheng L (2014) TOUGHREACT V3.0-OMP reference manual: a parallel simulation program for non-isothermal multiphase geochemical reactive transport. Berkeley, Calif

Yamamoto H, Zhang K, Karasaki K, Marui A, Uehara H, Nishikawa N (2009) Numerical investigation concerning the impact of CO_2 geologic storage on regional groundwater flow. Int J Greenhouse Gas Control 3:586–599

Yang Z, Niemi A, Tian L, Erlström M (2013a) Modelling of far-field pressure plumes for carbon dioxide sequestration. Energy Procedia, European Geosciences Union General Assembly 2013, EGUDivision Energy, Resources and the Environment, ERE, vol 40, pp 472–480

Yang Z, Tian L, Jung B, Joodaki S, Fagerlund F, Pasquali R, Vernon R, O'Neill N, Niemi A (2015) Assessing CO_2 storage capacity in the Dalders Monocline of the Baltic Sea Basin using dynamic models of varying complexity. Int J Greenhouse Gas Control 43:149–160

Yang Z, Tian L, Niemi A, Fagerlund F (2013b) Upscaling of the constitutive relationships for CO_2 migration in multimodal heterogeneous formations. Int J Greenhouse Gas Control 19:743–755

Yeh GT, Tsai CH (2013) HYDROGEOCHEM 6.0, a two-dimensional model of coupled fluid flow, thermal transport, HYDROGEOCHEMical transport, and geomechanics through multiple phase, systems version 6.0 (FACTM2D), theoretical basis and numerical approximation. Graduate Institute of Applied Geology, National Central University, Jhongli

Yortsos YC (1995) A theoretical analysis of vertical flow equilibrium. Transp Porous Media 18:107–129

Yortsos YC, Huang AB (1984) Linear stability analysis of immiscible displacement including continuously changing mobility and capillary effects: part I—simple basis flow profiles. Society of Petroleum Engineers, Dallas

Younes A, Ackerer P, Delay F (2010) Mixed finite elements for solving 2-D diffusion-type equations. Rev Geophys 48:rg1004

Zhang K, Wu YS, Pruess K (2008) User's guide for TOUGH2-MP—a massively parallel version of the TOUGH2 code (No. LBNL-315E). Lawrence Berkeley National Laboratory, Berkeley

Zhang L, Hou L, Wang L, Kan AT, Chen W, Tomson MB (2012) Transport of fullerene nanoparticles (nC60) in saturated sand and sandy soil: controlling factors and modeling. Environ Sci Technol 46:7230–7238

Zhao KXH, Wrobel LC, Power H (1995) Numerical simulation of viscous fingering using B-spline boundary elements. In: Wrobel LC, Brebbia CA (eds) Computational modeling of free and moving boundary problems II. Computational Mechanics, Southampton

Zhou Q, Birkholzer JT, Mehnert E, Lin Y-F, Zhang K (2010) Modeling basin- and plume-scale processes of CO_2 storage for full-scale deployment. Ground Water 48:494–514

Zoback MD, Gorelick SM (2015) To prevent earthquake triggering, pressure changes due to CO_2 injection need to be limited. Proc Natl Acad Sci 112:E4510

Zoback MD, Gorelick SM (2012) Earthquake triggering and large-scale geologic storage of carbon dioxide. Proc Natl Acad Sci 109:10164–10168